Accepted Manuscript

Numerical analysis of a finite element projection-based VMS turbulence model with wall laws

Tomás Chacón Rebollo, Macarena Gómez Mármol, Samuele Rubino

PII: S0045-7825(14)00449-6
DOI: http://dx.doi.org/10.1016/j.cma.2014.11.023
Reference: CMA 10473

To appear in: *Comput. Methods Appl. Mech. Engrg.*

Received date: 26 June 2014
Revised date: 9 November 2014
Accepted date: 13 November 2014

Please cite this article as: T. Chacón Rebollo, M. Gómez Mármol, S. Rubino, Numerical analysis of a finite element projection-based VMS turbulence model with wall laws, *Comput. Methods Appl. Mech. Engrg.* (2014), http://dx.doi.org/10.1016/j.cma.2014.11.023

- We develop a stabilized projection-based FE-VMS turbulence model including wall laws.
- We perform the numerical analysis of the model (stability, convergence, error estimates).
- We prove the asymptotic energy balance of the system for slightly smooth flows.
- Smooth flows are solved with optimal accuracy.
- Good accuracy is obtained with benchmark turbulent flow problems on coarse grids.

Numerical analysis of a finite element projection-based VMS turbulence model with wall laws

Tomás Chacón Rebollo [*], Macarena Gómez Mármol [†], Samuele Rubino [‡]

November 9, 2014

Abstract

This paper deals with the numerical analysis of a finite element projection-based VMS turbulence model that includes general non-linear wall laws. Only a single mesh and interpolation operators on a virtual coarser mesh are needed to implement the model. We include a projection-stabilization of pressure to use the same interpolation for velocity and pressure. Good accuracy is obtained with benchmark turbulent flow problems on coarse grids, that justify the interest of this approach. Also, the model solves smooth flows with optimal accuracy.

Keywords: Variational Multi-Scale Methods, Interpolation Operators, Wall Laws, Turbulence Modeling, Stabilized Methods, Numerical Analysis.

2010 Mathematics Subject Classification: 76D05, 76F06, 76N20, 65M60, 65M12.

1 Introduction

This paper deals with the numerical analysis of the approximation of incompressible flows in turbulent regime by means of the Variational Multi-Scale (VMS) models. The VMS models are increasingly used as a valid alternative to Large Eddy Simulation (LES) models, as they provide a similar accuracy and avoid some drawbacks. Indeed, no commutation error between the variational projection and differential operators occurs, that arises for LES models because the averaged/filtered equations do not satisfy the boundary conditions (Cf. [38, 39]). On the contrary, VMS are intrinsically discrete models, and no approximation of an intermediate averaged model is needed.

We focus here on the projection-based VMS-LES turbulence models (Cf. [33, 34, 35, 36]). These are three-level methods with large, sub-filter (resolved) scales and small un-resolved scales. The multi-scale setting clarifies the use of sub-grid eddy viscosity to model the viscosity interaction between the sub-filter scales and the small un-resolved scales. In particular, we will address a multi-scale Smagorinsky modeling of the eddy viscosity, which contains the restriction to the sub-filter scales through a projection/interpolation operator.

The simulation of wall-bounded flows with VMS models, however, may become very expensive in terms of computational resources due to the computation of boundary layers, as this requires very fine meshes in the normal direction to the wall (see, for instance, John

[*]Dpto. EDAN & IMUS, Universidad de Sevilla, C/Tarfia, s/n. 41012 Sevilla, Spain chacon@us.es
[†]Dpto. EDAN, Universidad de Sevilla, C/Tarfia, s/n. 41012 Sevilla, Spain macarena@us.es
[‡]Dpto. EDAN & IMUS, Universidad de Sevilla, C/Tarfia, s/n. 41012 Sevilla, Spain samuele@us.es

and Kindl [41], Bazilevs et al. [2]). A way to overcome this difficulty, recently applied to VMS models, is to weakly impose no-slip boundary conditions (Cf. [3, 4]). An alternative is the use of wall laws, which in their turn replace the usual no-slip boundary conditions by modeled conditions that set the stress of the flow at some distance from the wall. Wall laws are widely used in engineering simulation of turbulence, usually in RANS models. In this paper, we focus on the combined use of VMS-LES models with general non-linear wall-law boundary conditions, in the context of the Finite Element Method (FEM).

The most common wall law is the logarithmic law, introduced by Prandtl in 1925 (Cf. [49]), and derived by similarity laws by Von Karmán in 1930 (Cf. [58]). The mathematical and numerical analysis of wall laws, as boundary conditions for the Smagorkinsky LES turbulence model, was introduced by Parés (Cf. [47]). A serious difficulty linked to the approximation of wall laws is the discretization of slip boundary conditions. A strong imposition of these laws only applies to polyhedric domains. The more general treatment, introduced by Verfürth (Cf. [56, 57]), is by duality. This kind of discretization is quite involved, as it requires a specific boundary finite element space for the multipliers. In [48], Parés introduces a weak formulation of the slip condition. However, the analysis of these techniques has not been extended to mixed boundary conditions, in which other kinds of boundary conditions are imposed, in combination with wall laws, in different parts of the boundary. This is due to a lack of density results by smooth functions for the functional spaces involved. Here, we will analyze the case of mixed boundary conditions including wall laws, replacing the lacking density result by smooth functions by a similar one with finite element functions, for polyhedric domains.

In this paper, we perform the numerical analysis of a finite element projection-based VMS model that only needs a (fine) grid and interpolation operators on a virtual coarser grid. The large scales are represented in the coarse grid, while the sub-filter scales are their complement into the fine grid. The eddy diffusion term has a projection structure to filter out the large scales and let the eddy diffusion act only on the sub-filter resolved scales. We use high-order term-by-term stabilization to stabilize each single term that could lead to unstable discretizations (e.g. convection, pressure gradient), with high accuracy (Cf. [16, 17, 20]). This allows in particular to use polynomials of the same degree to interpolate velocity and pressure. The used stabilization procedure perfectly fits into the VMS framework. The model includes mixed Dirichlet - wall-law boundary conditions to take into account inflow and solid wall boundaries at the same time.

We perform a numerical analysis of this approximation in steady regime. We prove stability and weak convergence for solutions with the natural minimal regularity $(\mathbf{u}, p) \in [H^1(\Omega)]^3 \times L^2(\Omega)$. Moreover, we perform an error analysis, which strengthen the fact that the proposed model is suitable both for laminar and turbulent flows. In particular, for diffusion-dominated flows, we recover optimal convergence rates. The error analysis permits to prove the strong convergence of the proposed model for slightly smooth flows, and a subsequent asymptotic energy balance of the system. Finally, we perform numerical tests. On one hand, we show the good numerical performances of the proposed model confirming the theoretical convergence expectations for a 2D smooth steady flow (Test 1). On another hand, we present simulations of an equilibrium 3D channel flow at a friction-velocity Reynolds number $Re_\tau = 180$ on coarse grids, to analyze the basic numerical performances of the proposed model applied to the computation of turbulent flows, with and without wall-law boundary conditions (Test 2). Similar error levels are obtained for first and second-order statistics with respect to a residual-based VMS model on an equivalent coarse grid. The use of wall laws permits to maintain a similar good accuracy

(at least for the leading stream-wise velocity, as expected), with a significant reduction of the computational cost in comparison to the standard application of no-slip boundary conditions at the walls.

The structure of the paper is as follows: In Section 2, we present the variational formulation of the continuous and discrete problems we work with, and we state their main properties. Section 3 is devoted to the numerical analysis of the proposed discrete model (stability, convergence, error estimates), and to the study of the asymptotic energy balance of the system. The numerical tests are presented in Section 4. Finally, Section 5 states the main conclusions of the paper.

2 The continuous and discrete problems

We introduce a mixed boundary value problem for the steady incompressible Navier-Stokes equations, that includes a wall-law boundary condition in combination with an inflow boundary condition. Let Ω be a bounded polyhedric connected domain in $\mathbb{R}^d$, $d = 2$ or 3, with a Lipschitz boundary split into $\Gamma = \overline{\Gamma}_D \cup \overline{\Gamma}_n$. We suppose Γ split as the union of the sides $\Sigma_1, \ldots, \Sigma_r$, that we assume to be closed $(d-1)-$dimensional sets (straight segments when $d = 2$ or polygons when $d = 3$), in such a way that $\overline{\Gamma}_D = \bigcup_{i=1}^{k-1} \Sigma_i$, $\overline{\Gamma}_n = \bigcup_{i=k}^{r} \Sigma_i$, for some integer $k \in \{2, \ldots, r\}$.

We impose a Dirichlet inflow boundary condition on Γ_D and a wall-law boundary condition on Γ_n. The problem reads:

Find $\mathbf{u} : \Omega \longrightarrow \mathbb{R}^d$ *and* $p : \Omega \longrightarrow \mathbb{R}$ *such that:*

$$
(2.1) \qquad \left\{ \begin{array}{rcll} \nabla \cdot (\mathbf{u} \otimes \mathbf{u}) - 2\nu \nabla \cdot D(\mathbf{u}) + \nabla p &=& \mathbf{f} & \text{in } \Omega, \\ \nabla \cdot \mathbf{u} &=& 0 & \text{in } \Omega, \\ -\left[\mathbf{n} \cdot 2\nu D(\mathbf{u})\right]_\tau &=& \mathbf{g}(\mathbf{u})_\tau & \text{on } \Gamma_n, \\ \mathbf{u} \cdot \mathbf{n} &=& 0 & \text{on } \Gamma_n, \\ \mathbf{u} &=& \mathbf{u}_D & \text{on } \Gamma_D, \end{array} \right.
$$

where $\mathbf{u} \otimes \mathbf{u}$ is the tensor function of components $u_i u_j$, $D(\mathbf{u})$ is the symmetric deformation tensor given by $D(\mathbf{u}) = (1/2)(\nabla \mathbf{u} + (\nabla \mathbf{u})^t)$, $\mathbf{n}$ is the outer normal to Γ, the notation $_\tau$ represents the tangential component with respect to Γ defined as $\mathbf{u}_\tau = \mathbf{u} - (\mathbf{u} \cdot \mathbf{n})\mathbf{n}$, and $\mathbf{g} : \mathbb{R}^d \to \mathbb{R}^d$ is a given function, that determines the wall law (see below). The unknowns are the velocity $\mathbf{u}$ and the pressure p of the incompressible fluid. The data are the source term $\mathbf{f}$, that represents a body force per mass unit (typically the gravity), the kinematic viscosity ν of the fluid, that is a positive constant, and the Dirichlet data $\mathbf{u}_D$.

Remark 2.1. *The extension of the analysis performed in this paper to free-normal-tension (also called "do-nothing") boundary conditions on outflow boundaries is similar to the case of Navier-Stokes equations, with the essential difficulty of defining the proper projection operator to compute error estimates.*

Remark 2.2. *The analysis performed in the paper strongly uses the assumption that Ω is a polyhedric domain, to approximate the slip boundary condition $\mathbf{u} \cdot \mathbf{n} = 0$ on Γ_n. There exist well-established techniques to solve this difficulty for domain with curved boundaries, introduced by Verfürth. For instance, the slip condition may be considered as a restriction, and implemented through a saddle-point problem approach (Cf. [57]). Another possible remedy is to use isoparametric finite elements to fit the curved parts of the boundary (Cf. [56]). We do not consider here this situation, to avoid nonessential complexities that have been treated elsewhere.*

2.1 Variational formulation of the continuous problem

We consider the Sobolev spaces $H^s(\Omega)$, $s \in \mathbb{R}$, and $W^{m,p}(\Omega)$, $m \in \mathbb{N}$, $1 \leq p \leq \infty$, equipped with the standard norms. We denote by $||\cdot||_{m,p,\Omega}$ the standard norm in $W^{m,p}(\Omega)$. In order to give a variational formulation of problem (2.1), let us consider the velocity space:

$$\mathbf{W}(\Omega) = \left\{ \mathbf{w} \in [H^1(\Omega)]^d : \mathbf{w} = \mathbf{0} \text{ on } \Gamma_D, \mathbf{w} \cdot \mathbf{n} = 0 \text{ on } \Gamma_n \right\}.$$

This is a closed linear subspace of $[H^1(\Omega)]^d$, and thus a Hilbert space endowed with the $[H^1(\Omega)]^d$-norm. Indeed, it is well known that the trace is a continuous mapping from $H^1(\Omega)$ into $L^2(\Gamma)$. Also, the normal component of $\mathbf{w}$ exists a.e. on Γ, as $\mathbf{n} \in [L^\infty(\Gamma)]^d$, and since $\mathbf{w} \in [H^1(\Omega)]^d$, by trace theorem and Sobolev injection (Cf. [9]), its trace on Γ belongs to $[L^4(\Gamma)]^d$. Then, the mapping $\mathbf{w} \in \mathbf{W}(\Omega) \mapsto \mathbf{w} \cdot \mathbf{n} \in L^4(\Gamma_n)$ is continuous, as:

$$\|\mathbf{w} \cdot \mathbf{n}\|_{0,4,\Gamma_n} \leq \|\mathbf{w}\|_{0,4,\Gamma_n} \leq C \, \|\mathbf{w}\|_{1,2,\Omega}.$$

Thanks to Korn's inequalities (Cf. [32]), the $[H^1(\Omega)]^d$-norm is equivalent on $\mathbf{W}(\Omega)$ to the norm:

$$\|\mathbf{w}\|_{\mathbf{W}(\Omega)} = \|D(\mathbf{w})\|_{0,2,\Omega}.$$

We assume the Dirichlet boundary data admissible, in the sense that there exists a divergence-free lifting $\mathbf{U}_D \in [H^1(\Omega)]^d$ such that $\mathbf{U}_{D_{|\Gamma_D}} = \mathbf{u}_D$ and $\mathbf{U}_D = 0$ on $\overline{\Gamma}_n$. Such a lifting exists if $\mathbf{u}_D \in [H^{1/2}_{00}(\Gamma_D)]^d$, as we assume hereafter. In this way, we search for a continuous solution $\mathbf{u} = \mathbf{u}_0 + \mathbf{U}_D$, with $\mathbf{u}_0 \in \mathbf{W}(\Omega)$ divergence-free. We shall consider the following variational formulation of (2.1):

Find $(\mathbf{u}, p) \in [\mathbf{U}_D + \mathbf{W}(\Omega)] \times L^2_0(\Omega)$ *such that:*

$$\left\{ \begin{array}{rcl} b(\mathbf{u}; \mathbf{u}, \mathbf{v}) + a(\mathbf{u}, \mathbf{v}) - (p, \nabla \cdot \mathbf{v})_\Omega + \langle G(\mathbf{u}), \mathbf{v} \rangle & = & \langle \mathbf{f}, \mathbf{v} \rangle, \\ (\nabla \cdot \mathbf{u}, q)_\Omega & = & 0, \end{array} \right. \tag{2.2}$$

for any $(\mathbf{v}, q) \in \mathbf{W}(\Omega) \times L^2_0(\Omega)$, where $\langle \cdot, \cdot \rangle$ stands for the duality pairing between $\mathbf{W}(\Omega)$ and its dual $[\mathbf{W}(\Omega)]'$. The forms b, a and G are given by:

$$b(\mathbf{w}; \mathbf{u}, \mathbf{v}) = \frac{1}{2} \left[(\mathbf{w} \cdot \nabla \mathbf{u}, \mathbf{v})_\Omega - (\mathbf{w} \cdot \nabla \mathbf{v}, \mathbf{u})_\Omega \right], \tag{2.3}$$

$$a(\mathbf{u}, \mathbf{v}) = 2\nu \, (D(\mathbf{u}), D(\mathbf{v}))_\Omega, \tag{2.4}$$

$$\langle G(\mathbf{u}), \mathbf{v} \rangle = (\mathbf{g}(\mathbf{u}), \mathbf{v})_{\Gamma_n}, \tag{2.5}$$

for $\mathbf{u}$, $\mathbf{v}$, $\mathbf{w} \in [H^1(\Omega)]^d$. Semicolons $(;)$ are used for forms that are non-linear with respect to its first argument. The function g is given in implicit form as:

$$\mathbf{g}(\mathbf{u}) = \left\{ \begin{array}{ll} \dfrac{\mathbf{u}}{|\mathbf{u}|} (u_\tau)^2 & \text{if } |\mathbf{u}| > 0, \\ \\ \mathbf{0} & \text{if } |\mathbf{u}| = 0, \end{array} \right.$$

where $u_\tau = u_\tau(|\mathbf{u}|)$ is the wall-friction velocity, computed as unique solution of the algebraic equation:

$$u^+ = L(y^+), \text{ with } u^+ = \frac{|\mathbf{u}|}{u_\tau} \text{ and } y^+ = \frac{u_\tau y}{\nu}. \tag{2.6}$$

Here, u^+ is a friction non-dimensional velocity, L is the wall-law function, obtained from an asymptotic analysis in the boundary layer, y^+ denotes a friction non-dimensional normal

distance to the solid wall, and y denotes the normal distance to the solid wall. We suppose that the boundary layer is divided into two sub-layers (Cf. [21]):

$$T_1^+ = \Gamma_n \times [0, y_0^+], \quad T_2^+ = \Gamma_n \times [y_0^+, A^+],$$

where y_0^+ denotes a fixed friction non-dimensional normal distance to the solid wall. The most common wall-law function is the logarithmic law of Prandtl [49] and Von Kármán [58]:

$$L(y^+) = \begin{cases} y^+ & \text{if } y^+ \in [0, y_0^+], \\ \dfrac{1}{C_1}\log(y^+) + C_2 & \text{if } y^+ \in [y_0^+, A^+], \end{cases} \tag{2.7}$$

where $C_1 \simeq 0.41$ and $C_2 \simeq 5.5$ are constants, calculated from experimental measurements, and y_0^+ is chosen by preserving the continuity of L ($y_0^+ \simeq 11.5$). The law (2.7) does not take into account the transition zone between the viscous and logarithmic sub-layer, called the buffer layer. Actually, there exist other several possible settings of L (e.g., the Spalding's wall law [54]) which model the three boundary sub-layers by a single formula. In all cases, the wall-law function L is non-negative, strictly increasing and continuous, L' admits a finite number of discontinuities, and there exist two positive constants K_1 and K_2 such that:

$$\lim_{z^+ \to 0^+} \frac{L(z^+)}{z^+} = K_1, \quad \lim_{z^+ \to \infty} \frac{L(z^+)}{\log z^+} = K_2. \tag{2.8}$$

This ensures that the associated mapping G is well defined from $\mathbf{W}(\Omega)$ into its dual (Cf. Parés [47]).

2.2 Finite element spaces

This section focuses on the construction of finite element (FE) spaces that approximate the slip condition $\mathbf{u} \cdot \mathbf{n} = 0$ on Γ_n.

Let $\{\mathcal{T}_h\}_{h>0}$ be a family of affine-equivalent and conforming (i.e., without hanging nodes) triangulations of $\overline{\Omega}$, formed by triangles or quadrilaterals ($d = 2$), tetrahedra or hexaedra ($d = 3$). We shall assume that the family of triangulations $\{\mathcal{T}_h\}_{h>0}$ is also admissible in the following sense:

Definition 2.3. *The family of triangulations $\{\mathcal{T}_h\}_{h>0}$ is admissible if $\overline{\Gamma}_D$ and $\overline{\Gamma}_n$ are the union of whole sides of elements of $\mathcal{T}_h$.*

Given an integer $l \geq 0$, and an element $K \in \mathcal{T}_h$, denote by $\mathbb{R}_l(K)$ either $\mathbb{P}_l(K)$ (i.e., the space of Lagrange polynomials of degree $\leq l$, defined on K), if the grids are formed by triangles ($d = 2$) or tetrahedra ($d = 3$), or $\mathbb{Q}_l(K)$ (i.e., the space of Lagrange polynomials of degree $\leq l$ on each variable, defined on K), if the family of triangulations is formed by quadrilaterals ($d = 2$) or hexaedra ($d = 3$). We consider the following FE spaces for the velocity:

$$\begin{cases} Y_h^l = V_h^l(\Omega) = \{v_h \in C^0(\overline{\Omega}) : v_{h|_K} \in \mathbb{R}_l(K),\ \forall K \in \mathcal{T}_h\}, \\ \mathbf{Y}_h^l = [Y_h^l]^d = \{\mathbf{v}_h \in [C^0(\overline{\Omega})]^d : \mathbf{v}_{h|_K} \in [\mathbb{R}_l(K)]^d,\ \forall K \in \mathcal{T}_h\}, \\ \mathbf{X}_h = \{\mathbf{v}_h \in \mathbf{Y}_h^l : \mathbf{v}_h = \mathbf{0} \text{ on } \overline{\Gamma}_D, \mathbf{v}_h \cdot \mathbf{n}_i = 0 \text{ on } \Sigma_i, i = k, \ldots, r\} \subset \mathbf{Y}_h^l, \end{cases} \tag{2.9}$$

where $\mathbf{n}_i$ is the outer normal to Σ_i for $i = k, \ldots, r$, and we recall that $\overline{\Gamma}_n = \bigcup_{i=k}^{r} \Sigma_i$. Hereafter, $\mathbf{Y}_h^l$ (resp., Y_h^l) will constitute the discrete foreground vectorial (resp., scalar) spaces in which we will work on.

We prove that the family of spaces $\{\mathbf{X}_h\}_{h>0}$ is effectively an internal approximation of $\mathbf{W}(\Omega)$, i.e. a family of finite-dimensional sub-spaces of $\mathbf{W}(\Omega)$ such that for any $\mathbf{v} \in \mathbf{W}(\Omega)$:

$$\lim_{h \to 0} d_{1,2,\Omega}(\mathbf{v}, \mathbf{X}_h) = 0,$$

where:

$$d_{1,2,\Omega}(\mathbf{v}, \mathbf{X}_h) = \inf_{\mathbf{v}_h \in \mathbf{X}_h} \|\mathbf{v} - \mathbf{v}_h\|_{1,2,\Omega}.$$

To do it, let us consider the uniformly stable and convergent Bernardi-Maday-Rapetti (BMR, [6]) interpolation operator $\mathbb{P}_h$ from $[H^1(\Omega)]^d$ on $\mathbf{Y}_h^l$ as follows. Let us denote by $\mathcal{A}_h$ the set of Lagrange interpolation nodes for space $\mathbf{Y}_h^l$. Then:

$$\mathbb{P}_h \mathbf{v} = \sum_{\alpha \in \mathcal{A}_h} \overline{\mathbf{v}}_\alpha \, \lambda_\alpha(\mathbf{x}) \quad \text{for } \mathbf{x} \in \overline{\Omega}, \tag{2.10}$$

where λ_α are the canonic basis functions of the Lagrange interpolation, given by:

$$\lambda_\alpha \in Y_h^l, \quad \lambda_\alpha(\beta) = \delta_{\alpha,\beta} \quad \text{for all } \alpha, \beta \in \mathcal{A}_h,$$

with $\delta_{\alpha,\beta}$ the Kronecker delta and $\overline{\mathbf{v}}_\alpha$ an averaged value of $\mathbf{v}$ in a neighborhood of node α. Following Chacón and Lewandowski [22], Sect. A.3, it may be proved that if the family of triangulations is admissible, then the values $\overline{\mathbf{v}}_\alpha$ may be chosen to preserve both the no-slip and slip boundary conditions: If $\mathbf{v} \in \mathbf{W}(\Omega)$, then

$$\left\{ \begin{array}{rcl} \overline{\mathbf{v}}_\alpha \cdot \mathbf{n}_{|_F} & = & 0 \quad \text{for any } F \in \partial\mathcal{T}_h(\alpha) \text{ if } \alpha \in \mathcal{A}_h \cap \overline{\Gamma}_n, \\ \overline{\mathbf{v}}_\alpha & = & \mathbf{0} \quad \text{if } \alpha \in \mathcal{A}_h \cap \overline{\Gamma}_D, \end{array} \right.$$

where:

$$\partial\mathcal{T}_h(\alpha) = \{F \subset \Gamma \, : \, F \text{ is a side of some element of } \mathcal{T}_h \text{ such that } \alpha \in F \},$$

and $\mathbf{n}_{|_F}$ denotes the outer normal to Ω on F. This permits to prove the following:

Lemma 2.4. *Assume that the family of triangulations $\{\mathcal{T}_h\}_{h>0}$ is admissible. Then, $\mathbb{P}_h \mathbf{v} \in \mathbf{X}_h$ if $\mathbf{v} \in \mathbf{W}(\Omega)$.*

The proof of this Lemma can be found in [22], so that we omit it for brevity. Lemma 2.4 and the convergence in $H^1(\Omega)$ of the BMR interpolation operator $\mathbb{P}_h$ permits easily to conclude that the family $\{\mathbf{X}_h\}_{h>0}$ is an internal approximation of $\mathbf{W}(\Omega)$ for regular triangulations.

2.3 A projection-based VMS turbulence model

We approximate the weak formulation (2.2) of the boundary value problem (2.1) for the steady incompressible Navier-Stokes equations by a projection-based eddy viscosity multiscale model. To state it, let us introduce the space:

$$\overline{\mathbf{X}}_h = \{\mathbf{v}_h \in \mathbf{Y}_h^{l-1} : \mathbf{v}_h = \mathbf{0} \text{ on } \overline{\Gamma}_D, \mathbf{v}_h \cdot \mathbf{n}_i = 0 \text{ on } \Sigma_i, i = k, \ldots, r\}, \tag{2.11}$$

and consider a uniformly stable (in $H^1(\Omega)$-norm) interpolation operator Π_h on $\overline{\mathbf{Y}}_h$, where:

$$\overline{\mathbf{Y}}_h = [V_h^{l-1}(\Omega)]^d, \tag{2.12}$$

or:

$$\overline{\mathbf{Y}}_h = [V_H^{l}(\Omega)]^d, \tag{2.13}$$

and $V_H^l(\Omega)$ in (2.13) is a sub-space of $V_h^l(\Omega)$ with larger grid size $H > h$ (typically, $H = 2h$ or $H = 3h$). The considered interpolation operator Π_h must satisfy optimal error estimates (Cf. [6]), and preserve both the no-slip and slip boundary conditions when restricted to $\mathbf{X}_h$. Thus, we define:

$$\mathbf{X}'_h = (Id - \Pi_h)\mathbf{X}_h,$$

where Id is the identity operator. In accordance to (2.12), we identify $\overline{\mathbf{X}}_h = \Pi_h \mathbf{X}_h \subset \overline{\mathbf{Y}}_h = [V_h^{l-1}(\Omega)]^d$ as the large scales velocity space, and $\mathbf{X}'_h$ as the sub-filter scales velocity space. Space $\mathbf{X}'_h$ does not need to be explicitly constructed, only the operator Π_h is needed. In accordance to (2.13), another possible definition of $\overline{\mathbf{X}}_h$ is:

$$\overline{\mathbf{X}}_h = \{\mathbf{v}_h \in [V_H^l(\Omega)]^d : \mathbf{v}_h = \mathbf{0} \text{ on } \overline{\Gamma}_D, \mathbf{v}_h \cdot \mathbf{n}_i = 0 \text{ on } \Sigma_i, i = k, \ldots, r\}. \tag{2.14}$$

In practical implementations, we consider a standard nodal Lagrange interpolation operator Π_h for its simplicity and its efficiency with respect to other choices. This provides quite stable and accurate results. However, there exist other possibilities: we may mention the Scott-Zhang interpolation operator (Cf. [52]), or the already cited BMR (Cf. [6]). Also, the L^2-projection is used by John in [40] to define the large scales.

We state the projection-VMS discretization as:

Find $(\mathbf{u}_h, p_h) \in (\mathbf{U}_{Dh} + \mathbf{X}_h) \times \mathbb{M}_h$ *such that:*

$$\left\{ \begin{array}{rcl} b(\mathbf{u}_h; \mathbf{u}_h, \mathbf{v}_h) + a(\mathbf{u}_h, \mathbf{v}_h) + c'(\mathbf{u}_h; \mathbf{u}_h, \mathbf{v}_h) - (p_h, \nabla \cdot \mathbf{v}_h)_\Omega & + & \langle G(\mathbf{u}_h), \mathbf{v}_h \rangle \\ + s_{conv}(\mathbf{u}_h; \mathbf{u}_h, \mathbf{v}_h) & = & \langle \mathbf{f}, \mathbf{v}_h \rangle, \\ (\nabla \cdot \mathbf{u}_h, q_h)_\Omega + s_{pres}(p_h, q_h) & = & 0, \end{array} \right. \tag{2.15}$$

for any $(\mathbf{v}_h, q_h) \in \mathbf{X}_h \times \mathbb{M}_h$, where $\mathbf{X}_h$ is given by (2.9), and $\mathbb{M}_h = Y_h^l \cap L_0^2(\Omega)$, with $Y_h^l = V_h^l(\Omega)$ the foreground scalar space already given in (2.9). We search for a solution $\mathbf{u}_h = \mathbf{u}_{0h} + \mathbf{U}_{Dh}$, with $\mathbf{u}_{0h} \in \mathbf{X}_h$, and $\mathbf{U}_{Dh}$ the Stokes projection of $\mathbf{U}_D$ on $\mathbf{Y}_h^{l+1}$.

The form c' in (2.15) provides a multi-scale Smagorinsky modeling of the eddy viscosity (Cf. [53, 18]), given by:

$$c'(\mathbf{u}_h; \mathbf{u}_h, \mathbf{v}_h) = 2(\nu_T(\mathbf{u}'_h) D(\mathbf{u}'_h), D(\mathbf{v}'_h))_\Omega, \tag{2.16}$$

where:

$$\mathbf{u}'_h = \Pi_h^* \mathbf{u}_h, \quad \mathbf{v}'_h = \Pi_h^* \mathbf{v}_h, \quad \Pi_h^* = Id - \Pi_h,$$

and the eddy viscosity ν_T is defined as:

$$\nu_T(\mathbf{v})(\mathbf{x}) = (C_S h_K)^2 |D(\mathbf{v}_{|K})(\mathbf{x})| \quad \text{for } \mathbf{x} \in K, \tag{2.17}$$

where $|\cdot|$ denoties the Frobenius norm on $\mathbb{R}^{d \times d}$ and C_S is a (theoretically) universal constant. However, in practical applications, depending on the flow, the value of C_S may

vary between 0.065 (Cf. [45]) and 0.25 (Cf. [42]). Here, we shall use an intermediate value $C_S = 0.1$.

The forms s_{conv} and s_{pres} in (2.15) correspond to a high-order term-by-term stabilized method (Cf. [16, 17, 20]), and are given by:

$$s_{conv}(\mathbf{u}_h; \mathbf{u}_h, \mathbf{v}_h) = \sum_{K \in \mathcal{T}_h} \tau_{\nu,K}(\sigma_h^*(\mathbf{u}_h \cdot \nabla \mathbf{u}_h), \sigma_h^*(\mathbf{u}_h \cdot \nabla \mathbf{v}_h))_K,$$

$$s_{pres}(p_h, q_h) = \sum_{K \in \mathcal{T}_h} \tau_{p,K}(\sigma_h^*(\nabla p_h), \sigma_h^*(\nabla q_h))_K.$$

Here, $\tau_{\nu,K}$ and $\tau_{p,K}$ are stabilization coefficients for convection and pressure gradient, respectively, and $\sigma_h^* = Id - \sigma_h$, where σ_h is some locally stable (in $L^2(\Omega)$-norm) projection or interpolation operator on the foreground vectorial space $\mathbf{Y}_h^{l-1}$ (also called "buffer space" in this context), satisfying optimal error estimates. In practical implementations, we choose σ_h as a Scott-Zhang-like interpolation operator on space $\mathbf{Y}_h^{l-1}$ (Cf. [52]). This gives rise to a discretization with a reduced computational cost, but that maintains the same high-order accuracy with respect to standard projection-stabilized methods. For the subsequent numerical analysis, we need the following technical hypothesis on the stabilization coefficients:

Hypothesis 2.5. *The stabilization coefficients $\tau_{p,K}$ and $\tau_{\nu,K}$ satisfy the following condition:*

$$\alpha_1 h_K^2 \leq \tau_{p,K}, \tau_{\nu,K} \leq \alpha_2 h_K^2, \quad \forall K \in \mathcal{T}_h, \tag{2.18}$$

for some positive constants α_1 and α_2, independent of h.

We work with the following expression for the stabilization coefficients:

$$\tau_{p,K} = \tau_{\nu,K} = \left\{ \left[c_1 \frac{\nu + \overline{\nu}_{T|_K}}{(h_K/l)^2} \right] + \left[c_2 \frac{U_K}{(h_K/l)} \right] \right\}^{-1}, \tag{2.19}$$

by adapting the form of Codina (Cf. [24]). In (2.19), c_1 and c_2 are experimental positive constants, $\overline{\nu}_{T|_K}$ is some local eddy viscosity on element K, and U_K is some local speed on element K. We assume U_K uniformly bounded from below and from above for technical reasons. This ensures (2.18).

The term $\langle G(\mathbf{u}_h), \mathbf{v}_h \rangle$ in (2.15) corresponds to the imposition of wall-law boundary conditions. Note that we have neglected the small un-resolved scales in the modeling of wall laws. This is justified since wall laws apply to the mean flow, and we can identify it with the resolved flow. The rest of terms in (2.15) corresponds to a standard Galerkin discretization.

Formulation (2.15) is a projection-based VMS model for the steady incompressible Navier-Stokes equations (see [50] for its derivation). Following the standard VMS approach (Cf. [36]), the proposed model includes three grid levels: large resolved scales (those of $\overline{\mathbf{X}}_h$), small resolved (or sub-filter) scales (those of $\mathbf{X}'_h$), and small un-resolved scales. It is assumed that the interaction large-small un-resolved scales is weak whenever these are inside the inertial spectrum, so that it is neglected, while the action of small un-resolved scales on small resolved scales is modeled by a standard eddy viscosity plus a stabilization *ad-hoc* procedure. In particular, the form c' is referred to a sub-grid eddy viscosity term

that models the viscosity interaction between the sub-filter scales and small un-resolved scales.

The forms s_{conv} and s_{pres} are referred to the high-order term-by-term stabilization. This stabilization technique, that may be viewed somewhere between projection (Cf. [8, 25, 27]) and penalty (Cf. [13, 14]) stabilized methods, is usually applied to stabilize separately each single term (e.g., convection, pressure gradient) that could lead to unstable discretization with high accuracy, and permits to use equal interpolation for velocity and pressure. In this context, we propose to use the corresponding terms (as indeed are diffusive terms) with the aim to help to counter-balance the accumulation of sub-grid energy together with the sub-grid eddy viscosity term.

The proposed projection-based VMS turbulence model has thus a dual nature, as it results in a combination of (high-order term-by-term) stabilization and (projection) VMS-LES modeling. In this way, we almost recover one of the main feature of residual-based VMS methods (Cf. [2, 3, 25, 27]), since *on the one hand they are bona-fide LES-like turbulence models, and on the other hand they may be thought of as stabilized methods extended to the nonlinear realm* (from [3]). However, no eddy viscosity modeling is required by the residual-based VMS models, which are strongly consistent. Nevertheless, they result to be more complex with respect to the proposed model, which presents a simpler and less expensive structure for practical implementations such as to perform the numerical analysis.

3 Analysis of the discrete model

In this section, we perform the numerical analysis of model (2.15), that we will call in the sequel VMS-S model. For technical reasons, we assume throughout the work that the family of triangulations $\{\mathcal{T}_h\}_{h>0}$ is uniformly regular. Actually, this technical hypothesis may be relaxed to the more general case of regular grids, but we keep it to focus the analysis on the new aspects of the method, and to not unnecessarily lengthen it.

3.1 Technical background

We state in this subsection some technical results that are required for the numerical analysis. We shall denote throughout the paper by C_1, C_2, ... constants that may vary from a line to another, but which are always independent of h. We define the scalar products:

$$\begin{aligned} (\cdot,\cdot)_{\tau_p} : L^2(\Omega)\times L^2(\Omega) &\longrightarrow \mathbb{R}, \\ (f,g)_{\tau_p} &\longrightarrow \sum_{K\in\mathcal{T}_h} \tau_{p,K}(f,g)_K, \\ (\cdot,\cdot)_{\tau_\nu} : L^2(\Omega)\times L^2(\Omega) &\longrightarrow \mathbb{R}, \\ (f,g)_{\tau_\nu} &\longrightarrow \sum_{K\in\mathcal{T}_h} \tau_{\nu,K}(f,g)_K, \end{aligned}$$

and their associated norms:

$$||f||_{\tau_p} = (f,f)_{\tau_p}^{1/2}, \quad ||f||_{\tau_\nu} = (f,f)_{\tau_\nu}^{1/2}.$$

Lemma 3.1. *Assume that Hypothesis 2.5 holds. Then, the following conditions are satisfied:*

$$\forall z \in L^2(\Omega), \quad C_1 \sum_{K\in\mathcal{T}_h} h_K^2 ||z||_{0,2,K}^2 \le ||z||_\tau^2 \le C_2 \sum_{K\in\mathcal{T}_h} h_K^2 ||z||_{0,2,K}^2, \tag{3.1}$$

where τ denotes either τ_ν or τ_p, and:

$$\forall g \in L^2(\Omega), \quad ||\sigma_h^*(g)||_\tau \leq Ch||g||_{0,2,\Omega}. \tag{3.2}$$

Proof. Estimates (3.1) immediately follow from (2.18).
Let $g \in L^2(\Omega)$. By applying the second part of (3.1) to $\sigma_h^*(g)$, we obtain:

$$||\sigma_h^*(g)||_\tau^2 \leq C_2 \sum_{K\in\mathcal{T}_h} h_K^2 ||\sigma_h^*(g)||_{0,2,K}^2 \leq C_2 h^2 ||\sigma_h^*(g)||_{0,2,\Omega}^2 \leq Ch^2 ||g||_{0,2,\Omega}^2,$$

where we have used the global stability property of σ_h, due to the regularity of the mesh. Thus, we conclude $||\sigma_h^*(g)||_\tau \leq Ch||g||_{0,2,\Omega}$.

□

We next state a specific discrete inf-sup condition for the stabilized approximation, that is essential for the stability of method (2.15). The main difficulty in its proof stems from the fact that the interpolation operator σ_h takes value in $\mathbf{Y}_h^{l-1}$, thus reducing the effective number of degrees of freedom (d.o.f.) of the foreground velocity space $\mathbf{Y}_h^l$.

Lemma 3.2. *Assume that Hypothesis 2.5 holds. Then, we have the following inf-sup condition:*

$$\forall q_h \in \mathbb{M}_h, \quad ||q_h||_{0,2,\Omega} \leq C \left(\sup_{\mathbf{v}_h \in \mathbf{X}_h} \frac{|(\nabla \cdot \mathbf{v}_h, q_h)_\Omega|}{||D(\mathbf{v}_h)||_{0,2,\Omega}} + ||\sigma_h^*(\nabla q_h)||_{\tau_p} \right), \tag{3.3}$$

for some positive constant C independent of h.

The proof of this Lemma can be derived from [16]. Note that the discrete inf-sup condition (3.3) can be extended to a more complex condition that holds for a regular family of triangulations.

Our analysis also needs some properties of the eddy viscosity ν_T and the form c', that we state next.

Lemma 3.3. *There exists a constant $C > 0$ only depending on d, Ω and the aspect ratio of the family of triangulations such that:*

$$\|\nu_T(\mathbf{v}_h')\|_{0,\infty,\Omega} \leq C\, h^{2-d/2}\, \|D(\mathbf{v}_h)\|_{0,2,\Omega}, \tag{3.4}$$

$$|c'(\mathbf{v}_h; \mathbf{v}_h, \mathbf{w}_h)| \leq C\, h^{2-d/2}\, \|D(\mathbf{v}_h)\|_{0,2,\Omega}^2 \|D(\mathbf{w}_h)\|_{0,2,\Omega}. \tag{3.5}$$

Proof. As $\nabla \mathbf{v}_{h'}$ is piecewise discontinuous, then there exists $K \in \mathcal{T}_h$ such that:

$$\|\nu_T(\mathbf{v}_h')\|_{0,\infty,\Omega} = \|\nu_T(\mathbf{v}_h')\|_{0,\infty,K} \leq C_S^2\, h_K^2\, \|D(\mathbf{v}_h')\|_{0,\infty,K}.$$

By a local inverse estimate (Cf. [6]):

$$\|\nabla \mathbf{v}_h'\|_{0,\infty,K} \leq C\, h_K^{-d/2}\, \|\nabla \mathbf{v}_h'\|_{0,2,K},$$

for some constant $C > 0$ only depending on the aspect ratio of the family of triangulations. Then:

$$\begin{aligned} \|\nu_T(\mathbf{v}_h')\|_{0,\infty,\Omega} &\leq CC_S^2\, h_K^{2-d/2}\, \|D(\mathbf{v}_h')\|_{0,2,K} \leq C\, h^{2-d/2}\, \|D(\mathbf{v}_h')\|_{0,2,\Omega} \\ &\leq C\, h^{2-d/2}\, \|D((Id - \Pi_h)\mathbf{v}_h)\|_{0,2,\Omega} \leq C\, h^{2-d/2}\, \|D(\mathbf{v}_h)\|_{0,2,\Omega}, \end{aligned} \tag{3.6}$$

where the last inequality follows from the (H^1-)uniform stability property of the interpolation operator Π_h. By estimate (3.4) and the (H^1-)uniform stability of Π_h:

$$\begin{aligned} |c'(\mathbf{v}_h;\mathbf{v}_h,\mathbf{w}_h)| &\leq 2\|\nu_T(\mathbf{v}_h')\|_{0,\infty,\Omega}\,\|D(\mathbf{v}_h')\|_{0,2,\Omega}\|D(\mathbf{w}_h')\|_{0,2,\Omega} \\ &\leq C\,h^{2-d/2}\,\|D(\mathbf{v}_h)\|_{0,2,\Omega}^2\|D(\mathbf{w}_h)\|_{0,2,\Omega}. \end{aligned}$$

□

Also, the convection stabilizing term s_{conv} satisfies the following estimate:

Lemma 3.4. *Assume that Hypothesis 2.5 holds. Then:*

$$|s_{conv}(\mathbf{u}_h;\mathbf{u}_h,\mathbf{v}_h)| \leq Ch^{2-d/2}\|D(\mathbf{u}_h)\|_{0,2,\Omega}^3\|D(\mathbf{v}_h)\|_{0,2,\Omega}, \tag{3.7}$$

for some constant $C>0$ only depending on d, Ω and the aspect ratio of the family of triangulations.

Proof. By the definition of the form s_{conv}, we have:

$$\begin{aligned} |s_{conv}(\mathbf{u}_h;\mathbf{u}_h,\mathbf{v}_h)| &= \left|\sum_{K\in\mathcal{T}_h}\tau_{\nu,K}(\sigma_h^*(\mathbf{u}_h\cdot\nabla\mathbf{u}_h),\sigma_h^*(\mathbf{u}_h\cdot\nabla\mathbf{v}_h))_K\right| \\ &\leq C\sum_{K\in\mathcal{T}_h}h_K^2\|\sigma_h^*(\mathbf{u}_h\cdot\nabla\mathbf{u}_h)\|_{0,2,K}\|\sigma_h^*(\mathbf{u}_h\cdot\nabla\mathbf{v}_h)\|_{0,2,K}, \end{aligned}$$

where we have applied Hypothesis 2.5 and Cauchy-Schwarz inequality.
By using the (L^2-)local stability property of the interpolation operator σ_h, we obtain:

$$\begin{aligned} |s_{conv}(\mathbf{u}_h;\mathbf{u}_h,\mathbf{v}_h)| &\leq C\sum_{K\in\mathcal{T}_h}h_K^2\|\mathbf{u}_h\cdot\nabla\mathbf{u}_h\|_{0,2,\omega_K}\|\mathbf{u}_h\cdot\nabla\mathbf{v}_h\|_{0,2,\omega_K} \\ &\leq C\|\mathbf{u}_h\|_{0,4,\Omega}^2\sum_{K\in\mathcal{T}_h}h_K^2\|D(\mathbf{u}_h)\|_{0,4,\omega_K}\|D(\mathbf{v}_h)\|_{0,4,\omega_K}, \end{aligned}$$

where we have applied Hölder's inequality, and ω_K denotes the union of all elements of $\mathcal{T}_h$ that intersect K. By Sobolev embedding theorem, we can write:

$$\begin{aligned} |s_{conv}(\mathbf{u}_h;\mathbf{u}_h,\mathbf{v}_h)| &\leq C\|D(\mathbf{u}_h)\|_{0,2,\Omega}^2\sum_{K\in\mathcal{T}_h}h_K^2\|D(\mathbf{u}_h)\|_{0,4,\omega_K}\|D(\mathbf{v}_h)\|_{0,4,\omega_K} \\ &\leq C\|D(\mathbf{u}_h)\|_{0,2,\Omega}^2\sum_{K\in\mathcal{T}_h}h_K^{2-d/2}\|D(\mathbf{u}_h)\|_{0,2,\omega_K}\|D(\mathbf{v}_h)\|_{0,2,\omega_K}, \end{aligned}$$

where in the last inequality we have applied a local inverse estimate (Cf. [6]), and the local uniform regularity of the grid, which is implied by the regularity. Using again the regularity of the grid, which implies that $card(\omega_K)\leq N$ bounded for any K, we finally obtain:

$$\begin{aligned} &|s_{conv}(\mathbf{u}_h;\mathbf{u}_h,\mathbf{v}_h)| \\ &\leq Ch^{2-d/2}\|D(\mathbf{u}_h)\|_{0,2,\Omega}^2\left(\sum_{K\in\mathcal{T}_h}\|D(\mathbf{u}_h)\|_{0,2,\omega_K}\right)^{1/2}\left(\sum_{K\in\mathcal{T}_h}\|D(\mathbf{v}_h)\|_{0,2,\omega_K}\right)^{1/2} \\ &\leq Ch^{2-d/2}\|D(\mathbf{u}_h)\|_{0,2,\Omega}^3\|D(\mathbf{v}_h)\|_{0,2,\Omega}. \end{aligned}$$

□

We report now the properties of the mapping G, defined by (2.5), that sets the wall-law boundary condition in the steady incompressible Navier-Stokes equations (2.2) (Cf. [47]).

Lemma 3.5. *The functional G given by (2.5) is well defined from $\mathbf{W}(\Omega)$ into its dual, is monotone, compact, and satisfies the estimates: $\forall \mathbf{v}, \mathbf{w} \in \mathbf{W}(\Omega)$,*

$$\|G(\mathbf{v})\|_{[\mathbf{W}(\Omega)]'} \leq C\,(1 + \|\mathbf{v}\|^2_{1,2,\Omega}), \tag{3.8}$$

$$\|G(\mathbf{v}) - G(\mathbf{w})\|_{[\mathbf{W}(\Omega)]'} \leq C\,(1 + \|\mathbf{v}\|_{1,2,\Omega} + \|\mathbf{w}\|_{1,2,\Omega})\,\|\mathbf{v} - \mathbf{w}\|_{1,2,\Omega}, \tag{3.9}$$

where C is a positive constant only depending on d, Ω and Γ_n.

3.2 Existence and stability results

Problem (2.15) is equivalent to a system of algebraic non-linear equations in finite dimension. The non-linearity is due to several effects: the convection operator, the VMS-eddy viscosity, the convection stabilizing term, and the wall-law boundary condition. We use the Brouwer fixed point theorem to prove that it admits a solution (Cf. [9]). In particular, we have the following stability result:

Theorem 3.6. *Assume that Hypothesis 2.5 holds. Let $\mathbf{f} \in [\mathbf{W}(\Omega)]'$. Then, if $\|D(\mathbf{U}_D)\|_{0,2,\Omega}$ is small enough, problem (2.15) admits at least a solution, that satisfies the estimates:*

$$\|D(\mathbf{u}_{0h})\|_{0,2,\Omega} \leq C\left(\|\mathbf{f}\|_{[\mathbf{W}(\Omega)]'}; \|D(\mathbf{U}_D)\|_{0,2,\Omega}\right), \tag{3.10}$$

$$\|\sigma^*_h(\mathbf{u}_{0h} \cdot \nabla \mathbf{u}_{0h})\|_{\tau_\nu} + \|\sigma^*_h(\nabla p_h)\|_{\tau_p} \leq C\left(\|\mathbf{f}\|_{[\mathbf{W}(\Omega)]'}; \|D(\mathbf{U}_D)\|_{0,2,\Omega}\right), \tag{3.11}$$

$$\|p_h\|_{0,2,\Omega} \leq C\left(\|\mathbf{f}\|_{[\mathbf{W}(\Omega)]'}; \|D(\mathbf{U}_D)\|_{0,2,\Omega}\right), \tag{3.12}$$

where $C > 0$ is an increasing function of the data norms $\|\mathbf{f}\|_{[\mathbf{W}(\Omega)]'}$, $\|D(\mathbf{U}_D)\|_{0,2,\Omega}$, independent of h.

Proof. We prove the existence and stability of solutions in 4 steps.

Step 1: Linearization of (2.15).
Let $\mathbf{w}_h = \mathbf{w}_{0h} + \mathbf{U}_{Dh}$, with $\mathbf{w}_{0h} \in \mathbf{X}_h$ such that $\|D(\mathbf{w}_{0h})\|_{0,2,\Omega} \leq R$ (where R is a positive constant independent of h to be determined later), and consider the following linearized problem:

Given $\mathbf{f} \in [\mathbf{W}(\Omega)]'$, find $(\mathbf{u}_{0h}, p_h) \in \mathbf{X}_h \times \mathbb{M}_h$ such that:

$$B_T(\mathbf{w}_h, (\mathbf{u}_{0h}, p_h), (\mathbf{v}_h, q_h)) = \langle \widetilde{\mathbf{f}}, \mathbf{v}_h \rangle, \tag{3.13}$$

for all $(\mathbf{v}_h, q_h) \in \mathbf{X}_h \times \mathbb{M}_h$, where:

$$\begin{aligned} B_T(\mathbf{w}_h, (\mathbf{u}_{0h}, p_h), (\mathbf{v}_h, q_h)) &= b(\mathbf{w}_h, \mathbf{u}_{0h}, \mathbf{v}_h) + a(\mathbf{u}_{0h}, \mathbf{v}_h) + c'(\mathbf{w}_h, \mathbf{u}_{0h}, \mathbf{v}_h) \\ -(p_h, \nabla \cdot \mathbf{v}_h)_\Omega + \widehat{s}_{conv}(\mathbf{u}_{0h}, \mathbf{v}_h) &+ \langle \widehat{G}(\mathbf{u}_{0h}), \mathbf{v}_h \rangle + (\nabla \cdot \mathbf{u}_{0h}, q_h)_\Omega + s_{pres}(p_h, q_h), \end{aligned}$$

and:

$$\langle \widetilde{\mathbf{f}}, \mathbf{v}_h \rangle = \langle \mathbf{f}, \mathbf{v}_h \rangle - b(\mathbf{w}_h, \mathbf{U}_{Dh}, \mathbf{v}_h) - a(\mathbf{U}_{Dh}, \mathbf{v}_h) - c'(\mathbf{w}_h, \mathbf{U}_{Dh}, \mathbf{v}_h) - \widehat{s}_{conv}(\mathbf{U}_{Dh}, \mathbf{v}_h).$$

The symbol $\widehat{\ }$ denotes the linearization of the corresponding terms with respect to $\mathbf{w}_h$, i.e.:

$$\begin{aligned} \widehat{s}_{conv}(\mathbf{u}_{0h}, \mathbf{v}_h) &= \sum_{K \in \mathcal{T}_h} \tau_{\nu,K}(\sigma^*_h(\mathbf{w}_h \cdot \nabla \mathbf{u}_{0h}), \sigma^*_h(\mathbf{w}_h \cdot \nabla \mathbf{v}_h))_K, \\ \langle \widehat{G}(\mathbf{u}_{0h}), \mathbf{v}_h \rangle &= \int_{\Gamma_n} \mathbf{u}_{0h} \cdot \mathbf{v}_h\, e(|\mathbf{w}_h|)\, ds, \end{aligned}$$

where the function $e : \mathbb{R}_+ \to \mathbb{R}_+$ is defined by:

$$e(|\mathbf{u}|) = \begin{cases} \dfrac{[u_\tau(|\mathbf{u}|)]^2}{|\mathbf{u}|} & \text{if } |\mathbf{u}| > 0, \\ \dfrac{1}{(y/\nu)K_1} & \text{if } |\mathbf{u}| = 0, \end{cases} \tag{3.14}$$

and K_1 is given by (2.8). We recall that u_τ is the unique solution of the implicit equation (2.6). We prove that e is continuous. Indeed, let us re-write equation (2.6) as:

$$|\mathbf{u}| = u_\tau L(u_\tau y/\nu) = F(u_\tau).$$

The wall-law function L is strictly increasing and continuous, then F is strictly increasing and continuous. Due to (2.8), $\lim_{u_\tau \to 0^+} F(u_\tau) = 0$ and $\lim_{u_\tau \to \infty} F(u_\tau) = +\infty$. It implies that $u_\tau = F^{-1}(|\mathbf{u}|)$ is continuous, and so e is continuous at any $|\mathbf{u}| \neq 0$. To prove the continuity at $|\mathbf{u}| = 0$, we set $t = u_\tau(|\mathbf{u}|)$. Then, $|\mathbf{u}| = tL(\lambda t)$, with $\lambda = y/\nu$, and:

$$\lim_{|\mathbf{u}|\to 0} e(|\mathbf{u}|) = \lim_{t\to 0} \frac{t^2}{tL(\lambda t)} = \lim_{t\to 0} \frac{t}{L(\lambda t)} = \frac{1}{\lambda K_1},$$

where the last identity follows from (2.8). We deduce that $e(|\mathbf{w}_h|)$ is bounded on $\overline{\Omega}$:

$$\max_{\mathbf{x}\in\overline{\Omega}} e(|\mathbf{w}_h(\mathbf{x})|) \leq M(\|\mathbf{w}_h\|_{0,\infty,\Omega}), \text{ where } M(r) = \max_{x\in[0,r]} e(x).$$

The estimate for the form $\widehat{G}$ becomes:

$$\begin{aligned} \langle \widehat{G}(\mathbf{u}_{0h}), \mathbf{v}_h\rangle &\leq M(\|\mathbf{w}_h\|_{0,\infty,\Omega})\|\mathbf{u}_{0h}\|_{0,2,\Gamma_n}\|\mathbf{v}_h\|_{0,2,\Gamma_n} \\ &\leq CM(\|\mathbf{w}_h\|_{0,\infty,\Omega})\|D(\mathbf{u}_{0h})\|_{0,2,\Omega}\|D(\mathbf{v}_h)\|_{0,2,\Omega}. \end{aligned} \tag{3.15}$$

Step 2: Existence of solution of problem (3.13).
Problem (3.13) is equivalent to a linear system with $dim(\mathbf{X}_h) + dim(\mathbb{M}_h)$ unknowns and equations. Then, the existence of solutions is equivalent to its uniqueness. To prove uniqueness, let us assume that problem (3.13) admits a solution $(\mathbf{u}_{0h}, p_h) \in \mathbf{X}_h \times \mathbb{M}_h$, that we next estimate in terms of the data.

- Velocity estimate.

Take $\mathbf{v}_h = \mathbf{u}_{0h}$ and $q_h = p_h$ in (3.13) as test functions. This yields:

$$2\nu\|D(\mathbf{u}_{0h})\|^2_{0,2,\Omega} + c'(\mathbf{w}_h, \mathbf{u}_{0h}, \mathbf{u}_{0h}) + \widehat{s}_{conv}(\mathbf{u}_{0h}, \mathbf{u}_{0h}) + \langle \widehat{G}(\mathbf{u}_{0h}), \mathbf{u}_{0h}\rangle + s_{pres}(p_h, p_h) = \langle \widetilde{\mathbf{f}}, \mathbf{u}_{0h}\rangle,$$

as the form b is antisymmetric. Since the forms c' and $\widehat{G}$ are non-negative, we have:

$$2\nu\|D(\mathbf{u}_{0h})\|^2_{0,2,\Omega} + \widehat{s}_{conv}(\mathbf{u}_{0h}, \mathbf{u}_{0h}) + s_{pres}(p_h, p_h) \leq \langle \widetilde{\mathbf{f}}, \mathbf{u}_{0h}\rangle. \tag{3.16}$$

From the boundedness of the forms b and a in $[H^1(\Omega)]^d$, and (3.5), it follows:

$$\begin{aligned} \langle \widetilde{\mathbf{f}}, \mathbf{u}_{0h}\rangle \leq\ & (\|\mathbf{f}\|_{[\mathbf{W}(\Omega)]'} + \delta)\|D(\mathbf{u}_{0h})\|_{0,2,\Omega} + C_0 R\|D(\mathbf{U}_D)\|_{0,2,\Omega}\|D(\mathbf{u}_{0h})\|_{0,2,\Omega} \\ &+ C_1[diam(\Omega)]^{2-d/2}(R + \|D(\mathbf{U}_D)\|_{0,2,\Omega})\|D(\mathbf{U}_D)\|_{0,2,\Omega} + |\widehat{s}_{conv}(\mathbf{U}_{Dh}, \mathbf{u}_{0h})|, \end{aligned}$$

where $\delta = (C_0\|D(\mathbf{U}_D)\|_{0,2,\Omega} + 2\nu)\|D(\mathbf{U}_D)\|_{0,2,\Omega}$, and we have used $\|D(\mathbf{U}_{Dh})\|_{0,2,\Omega} \leq C\|D(\mathbf{U}_D)\|_{0,2,\Omega}$. By applying Hypothesis 2.5 and Young's inequality, we have:

$$|\widehat{s}_{conv}(\mathbf{U}_{Dh}, \mathbf{u}_{0h})| \leq C_2 \left(\sum_{K\in\mathcal{T}_h} \frac{h_K^2}{2} \|\sigma_h^*(\mathbf{w}_h \cdot \nabla \mathbf{U}_{Dh})\|_{0,2,K}^2 \right) + \frac{1}{2}\widehat{s}_{conv}(\mathbf{u}_{0h}, \mathbf{u}_{0h}) = I + II.$$

The second summand II passes to the left hand side of inequality (3.16). Using the (L^2-)local stability property of the interpolation operator σ_h on the first summand I, we obtain:

$$\begin{aligned} I &\leq C_3 \sum_{K\in\mathcal{T}_h} h_K^2 (\|\mathbf{w}_{0h} \cdot \nabla \mathbf{U}_{Dh}\|_{0,2,\omega_K}^2 + \|\mathbf{U}_{Dh} \cdot \nabla \mathbf{U}_{Dh}\|_{0,2,\omega_K}^2) \\ &\leq C_3 \sum_{K\in\mathcal{T}_h} h_K^2 (\|\mathbf{w}_{0h}\|_{0,\infty,\omega_K}^2 + \|\mathbf{U}_{Dh}\|_{0,\infty,\omega_K}^2) \|D(\mathbf{U}_{Dh})\|_{0,2,\omega_K}^2, \end{aligned}$$

where we have used Hölder's inequality in the last line. By a local inverse estimate (Cf. [6]), the regularity of the grid, and the Sobolev embedding theorem, we can write:

$$\begin{aligned} I &\leq C_4 \sum_{K\in\mathcal{T}_h} h_K^{2(1-d/4)} (\|\mathbf{w}_{0h}\|_{0,4,\omega_K}^2 + \|\mathbf{U}_{Dh}\|_{0,4,\omega_K}^2) \|D(\mathbf{U}_{Dh})\|_{0,2,\omega_K}^2 \\ &\leq C_5\, h^{2(1-d/4)} (R^2 + \|D(\mathbf{U}_D)\|_{0,2,\Omega}^2) \|D(\mathbf{U}_D)\|_{0,2,\Omega}^2 \leq M(R), \end{aligned}$$

with $M(R) = C_5\,[diam(\Omega)]^{2(1-d/4)}(R^2 + \|D(\mathbf{U}_D)\|_{0,2,\Omega}^2)\|D(\mathbf{U}_D)\|_{0,2,\Omega}^2$. Collecting all these estimates, from (3.16) we obtain:

$$\begin{aligned} & 2\nu\|D(\mathbf{u}_{0h})\|_{0,2,\Omega}^2 + \frac{1}{2}\widehat{s}_{conv}(\mathbf{u}_{0h}, \mathbf{u}_{0h}) + s_{pres}(p_h, p_h) \\ \leq & \left[\|\mathbf{f}\|_{[\mathbf{W}(\Omega)]'} + \widetilde{\delta}(R)\right] \|D(\mathbf{u}_{0h})\|_{0,2,\Omega} + M(R), \end{aligned}$$

where we have denoted:

$$\widetilde{\delta}(R) = \delta + \{C_0 R + C_1[diam(\Omega)]^{2-d/2}(R + \|D(\mathbf{U}_D)\|_{0,2,\Omega})\}\|D(\mathbf{U}_D)\|_{0,2,\Omega}.$$

Using Young's inequality:

$$\nu\|D(\mathbf{u}_{0h})\|_{0,2,\Omega}^2 + \frac{1}{2}\widehat{s}_{conv}(\mathbf{u}_{0h}, \mathbf{u}_{0h}) + s_{pres}(p_h, p_h) \leq \frac{\left[\|\mathbf{f}\|_{[\mathbf{W}(\Omega)]'} + \widetilde{\delta}(R)\right]^2}{4\nu} + M(R).$$

Finally, we conclude:

$$\|D(\mathbf{u}_{0h})\|_{0,2,\Omega} \leq \frac{\left[\|\mathbf{f}\|_{[\mathbf{W}(\Omega)]'} + \widetilde{\delta}(R)\right]}{2\nu} + \sqrt{\frac{M(R)}{\nu}}; \tag{3.17}$$

$$\|\sigma_h^*(\mathbf{w}_h \cdot \nabla \mathbf{u}_{0h})\|_{\tau_\nu} \leq \frac{\left[\|\mathbf{f}\|_{[\mathbf{W}(\Omega)]'} + \widetilde{\delta}(R)\right]}{\sqrt{2\,\nu}} + \sqrt{2\,M(R)}; \tag{3.18}$$

$$\|\sigma_h^*(\nabla p_h)\|_{\tau_p} \leq \frac{\left[\|\mathbf{f}\|_{[\mathbf{W}(\Omega)]'} + \widetilde{\delta}(R)\right]}{2\sqrt{\nu}} + \sqrt{M(R)}. \tag{3.19}$$

Observe that the bound (3.17) may be written as:

$$\|D(\mathbf{u}_{0h})\|_{0,2,\Omega} \leq \mathcal{K} + \frac{\mathcal{A}}{2}\|D(\mathbf{U}_D)\|_{0,2,\Omega} R, \tag{3.20}$$

with:

$$\mathcal{K} = \frac{\left[\|\mathbf{f}\|_{\mathbf{W}(\Omega)'} + \delta\right]}{2\nu} + \frac{\left(C_1 + 2\sqrt{C_5\nu}\right)\left[diam(\Omega)\right]^{2-d/2}}{2\nu}\|D(\mathbf{U}_D)\|_{0,2,\Omega}^2, \tag{3.21}$$

and:

$$\mathcal{A} = \frac{C_0 + \left(C_1 + 2\sqrt{C_5\nu}\right)\left[diam(\Omega)\right]^{2-d/2}}{\nu}. \tag{3.22}$$

As we want $\mathbf{w}_{0h}$ in the same ball of $\mathbf{u}_{0h}$, we impose $R = 2\mathcal{K}$, so that it must be:

$$\|D(\mathbf{u}_{0h})\|_{0,2,\Omega} \leq \mathcal{K} + \mathcal{A}\|D(\mathbf{U}_D)\|_{0,2,\Omega}\mathcal{K} \leq 2\mathcal{K}, \tag{3.23}$$

that is satisfied if:

$$\|D(\mathbf{U}_D)\|_{0,2,\Omega} \leq \mathcal{A}^{-1}.$$

- Pressure estimate.

Take $q_h = 0$ in (3.13). Using the previous estimates, this yields:

$$\begin{aligned} |(p_h, \nabla\cdot\mathbf{v}_h)_\Omega| &\leq |-\langle\widetilde{\mathbf{f}}, \mathbf{v}_h\rangle + b(\mathbf{w}_h, \mathbf{u}_{0h}, \mathbf{v}_h) + a(\mathbf{u}_{0h}, \mathbf{v}_h) + c'(\mathbf{w}_h, \mathbf{u}_{0h}, \mathbf{v}_h) \\ &+ \widehat{s}_{conv}(\mathbf{u}_{0h}, \mathbf{v}_h) + \langle\widehat{G}(\mathbf{u}_{0h}), \mathbf{v}_h\rangle| \\ \leq\ & C\left\{\|\widetilde{\mathbf{f}}\|_{[\mathbf{W}(\Omega)]'} + \left[1 + h^{2-d/2} + 2\nu + M(\|\mathbf{w}_h\|_{0,\infty,\Omega})\right]\|D(\mathbf{u}_{0h})\|_{0,2,\Omega}\right\}\|D(\mathbf{v}_h)\|_{0,2,\Omega} \\ \leq\ & C\left\{\|\widetilde{\mathbf{f}}\|_{[\mathbf{W}(\Omega)]'} + \left[1 + \nu + M(\|\mathbf{w}_h\|_{0,\infty,\Omega})\right]\mathcal{K}\right\}\|D(\mathbf{v}_h)\|_{0,2,\Omega}, \end{aligned}$$

where the second inequality follows from the boundedness of the forms b and a in $[H^1(\Omega)]^d$, and we have used properties (3.5), (3.7) and (3.15) to estimate respectively the forms c', $\widehat{s}_{conv}$ and $\widehat{G}$, while the last inequality follows from (3.23). By the discrete inf-sup condition (3.3) and (3.19), we obtain:

$$\begin{aligned} \|p_h\|_{0,2,\Omega} &\leq C\left(\sup_{\mathbf{v}_h\in\mathbf{X}_h}\frac{|(\nabla\cdot\mathbf{v}_h, p_h)_\Omega|}{\|D(\mathbf{v}_h)\|_{0,2,\Omega}} + \|\sigma_h^*(\nabla p_h)\|_{\tau_p}\right) \\ &\leq C\left\{\|\widetilde{\mathbf{f}}\|_{[\mathbf{W}(\Omega)]'} + \left[1 + \nu + \sqrt{\nu} + M(\|\mathbf{w}_h\|_{0,\infty,\Omega})\right]\mathcal{K}\right\}. \end{aligned}$$

Step 3: Existence of solution of problem (2.15).
We use Brouwer fixed point theorem to prove existence of solution of problem (2.15). Let us define the mapping $\mathcal{F} : \mathbf{X}_h \mapsto \mathbf{X}_h$, that transforms $\mathbf{w}_{0h} \in \mathbf{X}_h$ into $\mathbf{u}_{0h}$, the unique solution of problem (3.13). The previous estimates and the uniqueness of solution of (3.13) allow to prove the continuity of $\mathcal{F}$. Indeed, let $\{\mathbf{w}_n\}_{n\in\mathbb{N}} \subset \mathbf{X}_h$ be a sequence convergent to $\mathbf{w} \in [H^1(\Omega)]^d$. Let us consider the sequence of images $\{\mathcal{F}(\mathbf{w}_n)\}_{n\in\mathbb{N}} = \{\mathbf{u}_n\}_{n\in\mathbb{N}} \subset \mathbf{X}_h$. The previous estimates allow to extract a sub-sequence, that we denote in the same way, strongly convergent (as $\mathbf{X}_h$ is of finite dimension) to $\mathbf{t} \in \mathbf{X}_h$. Also, there exists a sub-sequence $\{p_n\}_{n\in\mathbb{N}} \subset \mathbb{M}_h$ strongly convergent to $p \in \mathbb{M}_h$. We take the limit $n \to +\infty$ in:

$$B_T(\mathbf{w}_n, (\mathbf{u}_n, p_n), (\mathbf{v}_h, q_h)) = \langle\widetilde{\mathbf{f}}, \mathbf{v}_h\rangle, \quad \forall(\mathbf{v}_h, q_h) \in \mathbf{X}_h \times \mathbb{M}_h.$$

Note that, as we are working in finite dimension, B_T is a continuous function, as all terms appearing in the definition of B_T are continuous functions of the d.o.f. of their arguments. We can conclude that:

$$B_T(\mathbf{w},(\mathbf{t},p),(\mathbf{v}_h,q_h)) = \langle \widetilde{\mathbf{f}}, \mathbf{v}_h \rangle, \quad \forall (\mathbf{v}_h,q_h) \in \mathbf{X}_h \times \mathbb{M}_h.$$

Thus, $\mathcal{F}(\mathbf{w}) = \mathbf{t}$. As the limit problem satisfied by $\mathbf{t}$ admits a unique solution, then the whole sequence $\{\mathcal{F}(\mathbf{w}_n)\}_{n\in\mathbb{N}}$ converges to it, by *reductio ad absurdum*. The previous estimates (3.23) also prove that $\mathcal{F}$ transforms the closed ball $\overline{B}_{\mathbf{X}_h}(0,2\mathcal{K})$ into itself. Then, by Brouwer fixed point theorem, the mapping $\mathcal{F}$ admits a fixed point. This fixed point is a solution of (2.15), satisfying the estimates (3.10), (3.11).

Step 4: Estimate (3.12).
It remains just to prove that the estimate for $\|p_h\|_{0,2,\Omega}$ does not depend on h for the non-linear problem (2.15). Note that the dependence on h in the linear case is due to estimate (3.15) of the form $\widehat{G}$, where M depends on $\|\mathbf{w}_h\|_{0,\infty,\Omega}$, and thus on h. Instead, in the non-linear case, we can directly apply (3.8) to estimate the form G, and thus the pressure estimate does not depend on h.

□

Remark 3.7. *The estimate (3.11) for the convective and pressure stabilizing terms guarantees an extra-control on the high frequencies of the convective derivative and pressure gradient, which is not obtained by standard projection-based VMS methods (Cf. [41]), for which only the sub-grid eddy viscosity term of Smagorinsky type is added to the standard Galerkin discretization.*

3.3 Convergence analysis

The convergence analysis is based upon the theory developed in [15], that enables to extend to stabilized methods the standard techniques for the numerical analysis of mixed methods.

We shall need a technical result that allows to represent formulation (2.2) as an internal approximation of an "augmented" variational formulation.

Definition 3.8. *A FE space $\mathbb{Z}_h$, constructed on a triangulation $\mathcal{T}_h$, is called a* **bubble FE space** *if, for all $b_h \in \mathbb{Z}_h$, for all $K \in \mathcal{T}_h$, $b_h \in H_0^1(K)$.*

A similar definition applies for vectorial bubble FE spaces.

Lemma 3.9. *There exists a family $\{\mathbb{Z}_h\}_{h>0}$ of bubble FE sub-spaces of $[H_0^1(\Omega)]^d$ and a family $\{\mathcal{S}_h\}_{h>0}$ of bilinear uniformly continuous and uniformly coercive forms on $[H_0^1(\Omega)]^d$ such that:*

$$s_{pres}(p_h,q_h) = \mathcal{S}_h(\mathcal{R}_h(\sigma_h^*(\nabla p_h)),\mathcal{R}_h(\sigma_h^*(\nabla q_h))), \quad \forall p_h,q_h \in \mathbb{M}_h, \tag{3.24}$$

where $\mathcal{R}_h : [H^{-1}(\Omega)]^d \longrightarrow \mathbb{Z}_h$ is the "static condensation" operator on $\mathbb{Z}_h$ defined as follows:

Given $\varphi \in [H^{-1}(\Omega)]^d$, $\mathcal{R}_h(\varphi)$ is the only element of $\mathbb{Z}_h$ that satisfies:

$$\mathcal{S}_h(\mathcal{R}_h(\varphi),z_h) = \langle \varphi, z_h \rangle, \quad \forall z_h \in \mathbb{Z}_h.$$

This result is proved in [15]. We shall also need the following property of bubble FE spaces (Cf. [15]):

Lemma 3.10. *If a sequence $\{\mathbb{Z}_h\}_{h>0}$ of bubble FE sub-spaces of $[H_0^1(\Omega)]^d$ is uniformly bounded in $[H_0^1(\Omega)]^d$, then it weakly converges to zero in $[H_0^1(\Omega)]^d$.*

We now state the weak convergence of solutions provided by method (2.15) to a weak solution of the Navier-Stokes boundary value problem (2.2).

Theorem 3.11. *Assume that Hypothesis 2.5 holds. Then, the sequence $\{(\mathbf{u}_h, p_h)\}_{h>0}$ of solutions of the VMS-S approximation (2.15) contains a sub-sequence which is weakly convergent in $[H^1(\Omega)]^d \times L^2(\Omega)$ to a solution of the steady Navier-Stokes equations (2.2). If this solution is unique, then the whole sequence converges to it.*

Proof. The proof is divided into various steps.

Step 1: Extracting sub-sequences.
Due to estimates (3.10)-(3.12), the sequence $\{(\mathbf{u}_{0h}, p_h)\}_{h>0}$ is uniformly bounded in the space $\mathbf{W}(\Omega) \times L_0^2(\Omega)$, which is a Hilbert space. Then, it contains a sub-sequence, that we still denote in the same way, weakly convergent in that space to some pair $(\mathbf{u}_0, p)$. As the injection of $H^1(\Omega)$ in $L^q(\Omega)$ is compact for $1 \leq q < q^* = 2d/(d-2)$, by the Rellich-Kondrachov compactness theorem (Cf. [9]) we may assume that the sub-sequence $\{\mathbf{u}_{0h}\}_{h>0}$ is strongly convergent in $[L^q(\Omega)]^d$, and so, in particular, in $[L^4(\Omega)]^d$. Also, the operator G is compact from $\mathbf{W}(\Omega)$ to its dual $[\mathbf{W}(\Omega)]'$, by Lemma 3.5. Then, we may assume that the sub-sequence $\{G(\mathbf{u}_{0h})\}_{h>0}$ is strongly convergent in $[\mathbf{W}(\Omega)]'$. We recall that $\mathbf{U}_{Dh}$ is the Stokes projection of $\mathbf{U}_D$ on $\mathbf{Y}_h^{l+1}$, thus it strongly converges to $\mathbf{U}_D$ in $[H^1(\Omega)]^d$. Let us prove that $(\mathbf{u}, p)$ is a solution of problem (2.2).

Step 2: Limit of convection terms.
Let us consider a pair of test functions $(\mathbf{v}, q)$ such that $\mathbf{v} \in \mathbf{W}(\Omega)$, $q \in \mathcal{D}(\Omega) \cap L_0^2(\Omega)$, where $\mathcal{D}(\Omega)$ is the space of $C_0^\infty(\Omega)-$functions (i.e., smooth functions with compact support in Ω), that is dense in $L^2(\Omega)$ (Cf. [44]). As $\mathbf{X}_h$ is an internal approximation of $\mathbf{W}(\Omega)$ (see Subsection 2.2), then there exists a sequence $\{\mathbf{v}_h\}_{h>0} \in \mathbf{X}_h$ strongly convergent to $\mathbf{v}$ in $\mathbf{W}(\Omega)$. Moreover, as $\mathbb{M}_h$ is an internal approximation of $H^1(\Omega) \cap L_0^2(\Omega)$, then there exists a sequence $\{q_h\}_{h>0} \in \mathbb{M}_h$ strongly convergent to q in particular in $L_0^2(\Omega)$. Then, it is standard to prove that:

$$\lim_{h\to 0} b(\mathbf{u}_h; \mathbf{u}_h, \mathbf{v}_h) = b(\mathbf{u}; \mathbf{u}, \mathbf{v}).$$

Moreover, by (3.7), for the convection stabilizing term we have:

$$|s_{conv}(\mathbf{u}_h; \mathbf{u}_h, \mathbf{v}_h)| \leq Ch^{2-d/2} \|D(\mathbf{u}_h)\|_{0,2,\Omega}^3 \|D(\mathbf{v}_h)\|_{0,2,\Omega}.$$

Since the sequences $\{\mathbf{u}_h\}_{h>0}$ and $\{\mathbf{v}_h\}_{h>0}$ are bounded in $[H^1(\Omega)]^d$, we deduce:

$$\lim_{h\to 0} s_{conv}(\mathbf{u}_h; \mathbf{u}_h, \mathbf{v}_h) = 0.$$

Step 3: Limit of diffusion terms.
As a is bilinear and continuous:

$$\lim_{h\to 0} a(\mathbf{u}_h, \mathbf{v}_h) = a(\mathbf{u}, \mathbf{v}).$$

Next, since the sequences $\{\mathbf{u}_h\}_{h>0}$ and $\{\mathbf{v}_h\}_{h>0}$ are bounded in $[H^1(\Omega)]^d$, we deduce from Lemma 3.3:

$$\lim_{h\to 0} c'(\mathbf{u}_h; \mathbf{u}_h, \mathbf{v}_h) = 0.$$

Step 4: Limit of pressure terms.
Since $\{\nabla\cdot\mathbf{u}_h\}_{h>0}$ is weakly convergent in $L^2(\Omega)$ to $\nabla\cdot\mathbf{u}$ and $\{q_h\}_{h>0}$ is strongly convergent in $L^2(\Omega)$ to q:

$$\lim_{h\to 0}(\nabla\cdot\mathbf{u}_h, q_h)_\Omega = (\nabla\cdot\mathbf{u}, q)_\Omega.$$

Also, we obviously have:

$$\lim_{h\to 0}(p_h, \nabla\cdot\mathbf{v}_h)_\Omega = (p, \nabla\cdot\mathbf{v})_\Omega.$$

The pressure stabilizing term also vanishes in the limit. To prove this, we use the representation formula (3.24). This yields:

$$\begin{aligned}\|\sigma_h^*(\nabla p_h)\|_{\tau_p}^2 = s_{pres,h}(p_h,p_h) &= \mathcal{S}_h(\mathcal{R}_h(\sigma_h^*(\nabla p_h)),\mathcal{R}_h(\sigma_h^*(\nabla p_h)))\\ &\geq \mu_S\|\mathcal{R}_h(\sigma_h^*(\nabla p_h))\|_{H_0^1(\Omega)}^2,\end{aligned}$$

using the uniform coercivity of the forms $\mathcal{S}_h$. Then, using the fact that $\|\sigma_h^*(\nabla p_h)\|_{\tau_p} \leq 2\sqrt{\nu}K$, we deduce that the sequence $\{\mathcal{R}_h(\sigma_h^*(\nabla p_h))\}_{h>0}$ is uniformly bounded in $[H_0^1(\Omega)]^d$ and, by Lemma 3.10, as:

$$s_{pres}(p_h,q_h) = \mathcal{S}_h(\mathcal{R}_h(\sigma_h^*(\nabla p_h)),\mathcal{R}_h(\sigma_h^*(\nabla q_h))) = \langle\sigma_h^*(\nabla q_h),\mathcal{R}_h(\sigma_h^*(\nabla p_h))\rangle,$$

we conclude:

$$\lim_{h\to 0} s_{pres}(p_h,q_h) = 0.$$

Consequently, the pair $(\mathbf{u},p)$ is a weak solution of the Navier-Stokes equations (2.2).

Step 7: Uniqueness.
As this weak convergence follows from a compactness argument, it is standard to prove, by *reductio ad absurdum*, that if the limit is unique, then the whole sequence converges to it, in the same weak sense.

□

Remark 3.12. *Following a standard strategy to prove the strong convergence of the velocities for the stabilized VMS-S method (2.15), one can only conclude:*

$$\lim_{h\to 0} 2\nu\|D(\mathbf{u}_{0h})\|_{0,2,\Omega}^2 + \|\sigma_h^*(\nabla p_h)\|_{\tau_p}^2 = 2\nu\|D(\mathbf{u}_0)\|_{0,2,\Omega}^2,$$

so that we cannot achieve a strong convergence result for solutions with natural minimal regularity, neither the corresponding asymptotic energy balance of the system (which is the case, instead, for mixed methods).

Remark 3.13. *Assuming a slightly increased regularity of the solution for the steady Navier-Stokes equations (2.1) leads to a strong convergence result also in the context of the stabilized VMS-S method (2.15) through an error estimates analysis (See Appendix). This will guarantee the corresponding asymptotic energy balance of the system, as we will state in the next subsection. Also, the error analysis performed in the Appendix proves that the convergence order of the VMS-S method (2.15) is optimal with respect to the polynomial interpolation for laminar smooth flows.*

3.4 Asymptotic energy balance

The error estimates result stated in Theorem 5.3 in Appendix, that implies the strong convergence in particular of the velocities (See Remark 5.4), contains as a sub-product the asymptotic energy balance of VMS-S model (2.15). Indeed, let us define the deformation energy E_D, the boundary friction energy E_F, the sub-grid eddy dissipation energy E_S, and the energy E_{SC} and E_{SP} respectively corresponding to the convection and the pressure stabilizing terms by:

$$\begin{aligned} E_D(\mathbf{u}) &= a(\mathbf{u},\mathbf{u}) &&= 2\nu\|D(\mathbf{u})\|^2_{0,2,\Omega}, \\ E_F(\mathbf{u}) &= \langle G(\mathbf{u}),\mathbf{u}\rangle &&= \int_{\Gamma_n} \mathbf{g}(\mathbf{u})\cdot\mathbf{u}\, ds, \\ E_S(\mathbf{u}_h) &= c(\mathbf{u}_h;\mathbf{u}_h,\mathbf{u}_h) &&= 2\sum_{K\in\mathcal{T}_h}(C_S h_K)^2 \int_K |D(\mathbf{u}_{h'})|^3\, d\mathbf{x}, \\ E_{SC}(\mathbf{u}_h) &= s_{conv,h}(\mathbf{u}_h;\mathbf{u}_h,\mathbf{u}_h) &&= \|\sigma_h^*(\mathbf{u}_h\cdot\nabla\mathbf{u}_h)\|^2_{\tau_\nu}, \\ E_{SP}(p_h) &= s_{pres,h}(p_h,p_h) &&= \|\sigma_h^*(\nabla p_h)\|^2_{\tau_p}. \end{aligned}$$

Then, it holds:

Corollary 3.14. *Let $\{(\mathbf{u}_h,p_h)\}_{h>0}$ be a sequence of solutions of the VMS-S model (2.15) strongly convergent in $[H^1(\Omega)]^d\times L^2(\Omega)$ to a solution $(\mathbf{u},p)$ of the Navier-Stokes equations (2.2) with regularity $[H^2(\Omega)]^d\times H^1(\Omega)$ (at least). Then:*

$$\lim_{h\to 0}[E_D(\mathbf{u}_h)+E_F(\mathbf{u}_h)+E_S(\mathbf{u}_h)+E_{SC}(\mathbf{u}_h)+E_{SP}(p_h)] = E_D(\mathbf{u})+E_F(\mathbf{u}),$$

as:

$$\lim_{h\to 0} E_D(\mathbf{u}_h) = E_D(\mathbf{u}), \quad \lim_{h\to 0} E_F(\mathbf{u}_h) = E_F(\mathbf{u}),$$

and:

$$\lim_{h\to 0} E_S(\mathbf{u}_h) = \lim_{h\to 0} E_{SC}(\mathbf{u}_h) = \lim_{h\to 0} E_{SP}(p_h) = 0.$$

Thus, the total energy balance is asymptotically maintained in such a way that the deformation energy and the energy dissipated at the wall pass to the limit. In addition, the dissipated eddy energy so as the sub-grid energy due to stabilizing terms asymptotically vanish.

4 Numerical examples

We have performed numerical experiments by using the projection-based VMS model (2.15), on one hand to test the theoretical convergence order predicted by the numerical analysis, and stated in Appendix (Theorem 5.3). This is performed in Test 1, where we have considered a 2D smooth steady flow with analytical solution to check the expected optimal convergence order with respect to the polynomial interpolation. On another hand, to analyze the basic numerical performances of the proposed model applied to the computation of turbulent flows, with and without wall-law boundary conditions. This is performed in Test 2, where we address simulations of a fully developed 3D turbulent channel flow at $Re_\tau = 180$, for which there exists an extensive literature providing reliable numerical results.

4.1 Test 1: Convergence order

This test is aimed to confirm the optimal convergence order of model (2.15) for laminar smooth flows. We have considered a 2D steady flow in the domain $\Omega = (0, \pi)^2$, whose analytical solution is given by:

- Horizontal velocity: $u_1 = 2(\sin x_1)^2 \sin x_2 \cos x_2$;
- Vertical velocity: $u_2 = -2 \sin x_1 (\sin x_2)^2 \cos x_1$;
- Pressure: $p = \cos x_1 \cos x_2$.

The velocity field vanishes on $\partial\Omega$. As physical property, we have taken $\nu = 10^{-2}$. The force term $\mathbf{f}$ is computed to match the exact solution. We have used regular meshes with grid size h ranging from 0.9 to 0.06, and triangular finite elements of degree 2, 3, and 4 for velocity and pressure ($l = 2, 3, 4 =$ degree of the polynomial interpolation). We have used setting (2.17) for the multi-scale eddy viscosity term, with nodal interpolation operator Π_h taking values in $\overline{\mathbf{Y}}_h$ defined by (2.12). In this way, only a single mesh is needed for implementation. The stabilization coefficients are given by the adapted Codina's form (2.19), with constants $c_1 = 4$, $c_2 = \sqrt{c_1} = 2$ (Cf. [26]).

In Figure 1, we have plotted the slopes of the estimated error curves for the velocity (in H^1-norm) and the pressure (in L^2-norm), related to the grid size h. We observe that the convergence rate is optimal, so that we obtain an excellent agreement with respect to the theoretical predictions.

4.2 Test 2: Turbulent channel flow

The 3D channel flow is one of the most popular test problems for the investigation of wall bounded turbulent flows. It was pioneered as a LES test problem by Moin and Kim (Cf. [45]), and more recently has been extensively used to test several versions of LES models. Let us mention, for instance, the simulation carried out by Iliescu and Fischer [37] using a Rational LES (RLES) model, in the context of a spectral element code. A number of numerical studies on turbulent channel flow has also been performed applying VMS methods. Among others, Bazilevs et al. [2] tested a Residual-based VMS (RB-VMS) turbulence model on a channel flow, employing linear, quadratic and cubic NURBS (Non-Uniform Rational B-Splines), while John and Kindl [41] compared the performances of two types of VMS methods, where one uses bubble functions to model resolved small scales (Residual Free Bubble-based method), whereas the other one contains the definition of the resolved small scales by an explicit projection in its set of equations (Projection-based method). For the setup of our numerical simulations, we choose to follow the guidelines given by Gravemeier in [30], where different scale-separating operators for a VMS-LES of a turbulent channel flow in the context of a Finite Volume Method (FVM) are tested.

As a benchmark, we will use the fine Direct Numerical Simulation (DNS) of Moser, Kim and Mansour [46].

- Setup for numerical simulations.

We test model (2.15) with the following different settings of the eddy viscosity term:

- SMA model: The Smagorinsky setting, given by

$$c'(\mathbf{u}_h; \mathbf{u}_h, \mathbf{v}_h) = 2(\nu_T(\mathbf{u}_h) D(\mathbf{u}_h), D(\mathbf{v}_h))_\Omega;$$

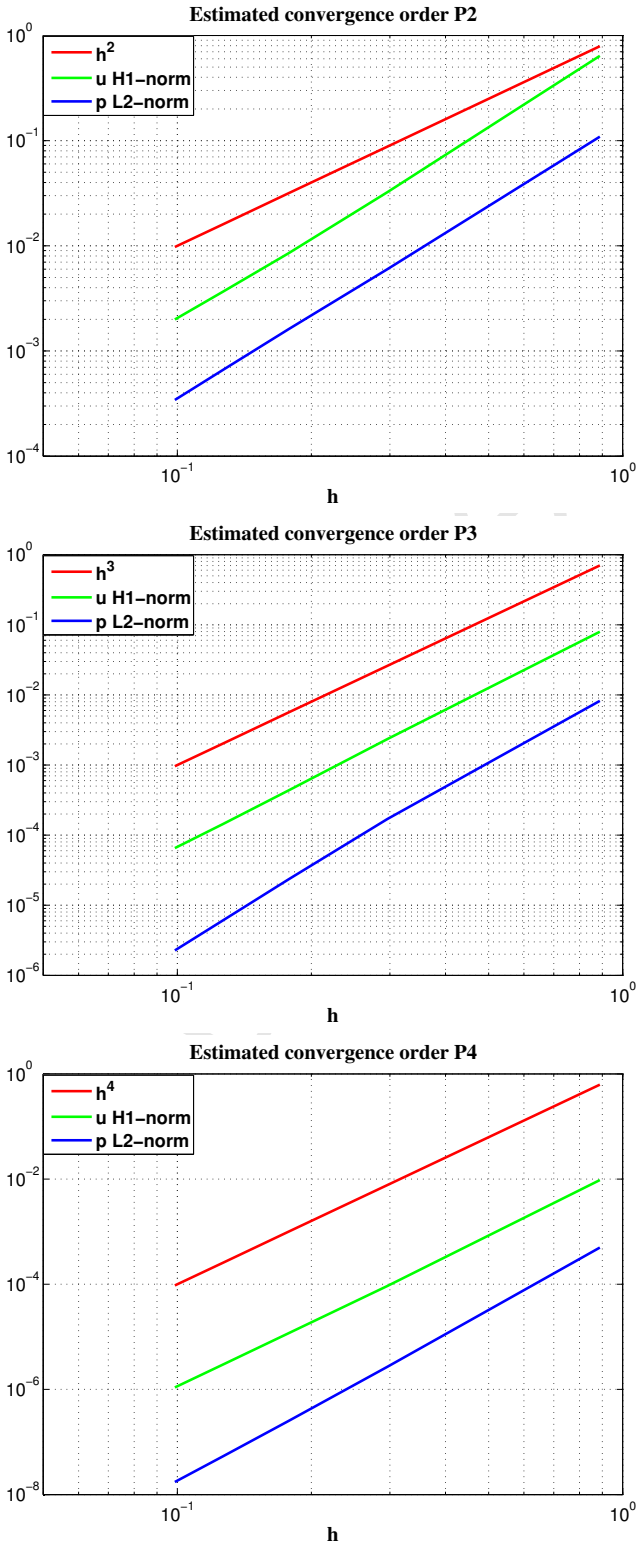

Figure 1:
Estimated convergence orders using $P2$, $P3$, and $P4$ FE for velocity and pressure.

- VMS-S model: The *Small-Small* VMS-Smagorinsky setting, given by

$$c'(\mathbf{u}_h;\mathbf{u}_h,\mathbf{v}_h) = 2(\nu_T(\mathbf{u}'_h)D(\mathbf{u}'_h), D(\mathbf{v}'_h))_\Omega;$$

- VMS-B model: The Berselli-Iliescu-Layton setting of Ref. [7], in which:

$$c'(\mathbf{u}_h;\mathbf{u}_h,\mathbf{v}_h) = 2(\nu_T(\widetilde{\Pi}_h^* D(\mathbf{u}_h))\widetilde{\Pi}_h^* D(\mathbf{u}_h), \widetilde{\Pi}_h^* D(\mathbf{v}_h))_\Omega,$$

where $\widetilde{\Pi}_h^* = Id - \widetilde{\Pi}_h$, and we have denoted by $\widetilde{\Pi}_h$ the $[L^2(\Omega)]^{d\times d}$-orthogonal projection on the space:

$$L_h = D(\overline{\mathbf{Y}}_h) = \{d_h \in [L^2(\Omega)]^{d\times d} : d_h = D(\overline{\mathbf{w}}_h), \text{ for some } \overline{\mathbf{w}}_h \in \overline{\mathbf{Y}}_h\}.$$

In the numerical experiments, we perform simulations with a slight modification of this method, where we replace the $[L^2(\Omega)]^{d\times d}$-orthogonal projection $\widetilde{\Pi}_h$ on space L_h by an interpolation operator on a coarser (e.g., $P0$) FE space, much faster to compute.

We use a setup similar to the one of Gravemeier [30]. The computational domain is $\Omega = (0, L_1) \times (-\delta, \delta) \times (0, L_3)$, with $\delta = 1$ (wall-normal direction), $L_1 = 2\pi$ (stream-wise direction), and $L_3 = (4/3)\pi$ (span-wise direction). The boundary conditions are periodic in both the stream-wise and span-wise directions, commonly referred to as homogeneous directions. We perform a comparison between the application of no-slip and wall-law boundary conditions at the walls. The viscosity is $\nu = 1/180 = 5.5 \times 10^{-3}$. The turbulent wall-shear velocity $u_\tau = \sqrt{\tau}$, where τ denotes the wall-shear stress, and the channel half-width δ define the Reynolds number:

$$Re_\tau = \frac{u_\tau\,\delta}{\nu},$$

besides the kinematic viscosity ν. The Reynolds number based on a unit friction velocity reachable at a steady state is $Re_\tau = 180$.

Our strategy is as follows: to reach a statistically steady state, we use an evolution approach starting by an initial parabolic velocity profile perturbed by a random velocity fluctuation. We first run a simulation with no-slip boundary conditions at the walls, in order to stabilize u_τ near a unitary value. Random velocity fluctuations of 10%-amplitude of the bulk mean stream-wise velocity perturbs the initial condition for the velocity field:

$$\begin{cases} u_1(y, t=0) &= u_{1,c}(1-y^2) + 0.1u_{1,m}\psi_{ran}, \\ u_2(y, t=0) &= 0.1u_{1,m}\psi_{ran}, \\ u_3(y, t=0) &= 0.1u_{1,m}\psi_{ran}, \end{cases}$$

where $u_{1,c}$ denotes the stream-wise velocity at the centerline of the channel, $u_{1,m}$ the bulk mean stream-wise velocity, and $\psi_{ran} \in [-1, 1]$ a random number. We choose $u_{1,c} = 25$, and hence $u_{1,m} = \int_0^\delta u_{1,c}(1-y^2)dy = 2u_{1,c}/3 = 16.7$. So, the corresponding Reynolds number based on the bulk mean stream-wise velocity ($Re_m = u_{1,m}2\delta/\nu$, see [43]) is $Re_m = 6\,012$. The flow is driven by a constant forcing $\mathbf{f} = (f_p, 0, 0) = (1, 0, 0)$, that models an imposed pressure gradient in the stream-wise direction. The specific choice of a unit value for f_p aims at obtaining a unit value for u_τ in the statistically steady state, subject to the relation $u_\tau = \sqrt{f_p\delta}$ (Cf. [29]). We choose to work with Van Driest Damping [55], so that the Smagorinsky constant is changed to the expression $C_S(1 - \exp(-y^+/A^+))$, where

$C_S = 0.1$ according to the original choice in [28], $y^+ = (\delta - |y|)u_\tau/\nu$ is the non-dimensional distance from the wall, and $A^+ = 26$ is the Van Driest constant.

The difficulty we face in the numerical simulations is to obtain a good accuracy with a relatively coarse spatial resolution. Our grid consists of a 16^3 partition of the channel, uniform in the homogeneous directions. The distribution of nodes in the wall-normal direction is non-uniform, and obeys the cosine function of Gauss-Lobatto:

$$y_i = -\cos\left(\frac{i\pi}{N_y}\right), \quad i = 0, \ldots, N_y = 16.$$

We use three-dimensional $P2$ FE for velocity and pressure. These choices give rise to 4 096 mesh cells (i.e., 24 576 tetrahedra), 33 792 d.o.f. for each scalar variable, and a distance of the d.o.f. next to the walls $y^+_{min} = 1.7293$. In Gravemeier [30], a VMS-Smagorinsky model, based on projection/averaging operators and the use of two nested meshes, is used in a FVM with 32 control volumes in all coordinate directions for Reynolds number $Re_\tau = 180$. A simulation equivalent in number of d.o.f. to our discretization for a turbulent channel flow at $Re_\tau = 180$ has been carried out by Akkerman in his PhD thesis [1], by using a RB-VMS turbulence model. Indeed, his coarsest computation consists on Q_1 FE applied on a 32^3 partition of the computational domain, that results in a number of d.o.f. equivalent to our value, obtained by using $P2$ FE on a 16^3 partition of the channel. Note that the data from the fine DNS of Moser, Kim and Mansour [46] are obtained by a subdivision of the channel of 128^3.

We use the Crank-Nicolson scheme for the temporal discretization, combined with linearization of convective and sub-grid eddy viscosity terms. The choice of this modified Crank-Nicolson scheme is due to the fact that it provides a good compromise between accuracy and computational complexity, while keeping the numerical diffusion levels below the sub-grid terms (Cf. [41]). To run the first part of simulation, we solve in practice the following linearized system in each time step:

$$\text{(4.1)} \qquad \begin{cases} \left(\dfrac{\mathbf{u}_h^{n+1} - \mathbf{u}_h^n}{\Delta t}, \mathbf{v}_h\right)_\Omega + b(\mathbf{u}_h^n, \mathbf{u}_h^{n+\theta}, \mathbf{v}_h) + a(\mathbf{u}_h^{n+\theta}, \mathbf{v}_h) & + & c'(\mathbf{u}_h^n, \mathbf{u}_h^{n+\theta}, \mathbf{v}_h) \\ \qquad -(p_h^{n+\theta}, \nabla \cdot \mathbf{v}_h)_\Omega + \widehat{s}_{conv}(\mathbf{u}_h^{n+\theta}, \mathbf{v}_h) & = & \langle \mathbf{f}, \mathbf{v}_h \rangle, \\ (\nabla \cdot \mathbf{u}_h^{n+\theta}, q_h)_\Omega + \widetilde{s}_{pres}(p_h^{n+\theta}, q_h) + \varepsilon(p_h^{n+1}, q_h)_\Omega & = & 0, \end{cases}$$

where:

$$\mathbf{u}_h^{n+\theta} = \theta \mathbf{u}_h^{n+1} + (1-\theta)\mathbf{u}_h^n, \quad p_h^{n+\theta} = \theta p_h^{n+1} + (1-\theta)p_h^n, \quad \theta = 1/2.$$

In (4.1), the form c' denotes the linearized (with respect to the convection velocity at a previous time step $\mathbf{u}_h^n$) eddy diffusion term defined by either VMS-S, VMS-B or SMA models, and the term with factor ε denotes a penalty term, that permits to fix the constant the pressure is determined up through the formulation, for a small positive value of ε (e.g., $\varepsilon = 10^{-10}$ in the numerical simulations). The stabilizing terms are defined by:

$$\text{(4.2)} \qquad \widehat{s}_{conv}(\mathbf{u}_h^{n+\theta}, \mathbf{v}_h) = \sum_{K \in \mathcal{T}_h} (\tau^n_{\nu,K}\, \sigma^*_h(\mathbf{u}_h^n \cdot \nabla \mathbf{u}_h^{n+\theta}), \sigma^*_h(\mathbf{u}_h^n \cdot \nabla \mathbf{v}_h)),$$

$$\text{(4.3)} \qquad \widetilde{s}_{pres}(p_h^{n+\theta}, q_h) = \sum_{K \in \mathcal{T}_h} (\tau^n_{p,K}\, \widetilde{\sigma}^*_h(\nabla p_h^{n+\theta}), \widetilde{\sigma}^*_h(\nabla q_h)),$$

where $\widetilde{\sigma}_h^* = Id$. Due to the low regularity of the pressure and the use of coarse meshes, the choice $\widetilde{\sigma}_h^* = \sigma_h^*$ gives rise to small numerical instabilities during the computation for this test, that lead in practice to oscillating numerical results, even if with small amplitude (we have stability in L^2-norm, but not in L^∞). The oscillations shall decrease by reducing the grid size. Therefore, a way to avoid them is to take local averages in space of the pressure. Here, we prefer to not consider the projection-based pressure stabilization (overall method of first order), which provides no oscillations, maintaining similar error levels for turbulent flows. The stabilization coefficients are given by the adapted Codina's form (2.19):

$$\tau_{p,K}^n = \tau_{\nu,K}^n = \left\{ \left[c_1 \frac{\nu + \overline{\nu}_{T|_K}^n}{(h_K/2)^2} \right] + \left[c_2 \frac{U_K^n}{(h_K/2)} \right] \right\}^{-1},$$

where $U_K^n = \|\mathbf{u}_h^n\|_{0,2,K}/|K|^{1/2}$, and $\overline{\nu}_{T|_K}^n = (C_S h_K)^2 U_K^{*,n}$, with:

- $U_K^{*,n} = \|D(\Pi_h^* \mathbf{u}_h^n)\|_{0,2,K}/|K|^{1/2}$ for the VMS-S model;
- $U_K^{*,n} = \|\widetilde{\Pi}_h^* D(\mathbf{u}_h^n)\|_{0,2,K}/|K|^{1/2}$ for the VMS-B model;
- $U_K^{*,n} = \|D(\mathbf{u}_h^n)\|_{0,2,K}/|K|^{1/2}$ for the SMA model.

The value for the constants c_1 and c_2 are $c_1 = 4$, $c_2 = \sqrt{c_1} = 2$ (Cf. [26]). For simplicity of implementation, we define the element size $h_K = \sqrt[3]{|K|}$, for all $K \in \mathcal{T}_h$. Problem (4.1) is implemented on a FreeFem++ (Cf. [31]) numerical code (published in [22]), and the corresponding system is solved by a GMRES (Generalized Minimal Residual) method (Cf. [51]). The same numerical code [19] has been already used in [5] to perform the same experiment with a similar discretization but involving boundary conditions on the pressure to model the pressure jump that drives the flow between inflow and outflow boundaries, instead of the forcing term imposed in this work. The simulation results are very similar, thus stressing the robustness of the code.

The discretized scheme (4.1) is first integrated for 1250 time steps, with $\Delta t = 0.004$. This time step is smaller than the Kolmogorov time scale, and it fits into the range proposed in [23] to ensure numerical stability (Cf. [41]). Within this time period, the flow is expected to develop to full extent, including a subsequent relaxation time. Note that, on one hand, without adding the stabilizing terms (4.2) and (4.3), method (4.1) results to be clearly unstable for the numerical simulation considered (in particular, it is not possible to stabilize the wall-shear velocity u_τ near a unitary value, since we experience a blow-up in finite time). On another hand, in the computations, we have also analyzed the performance of method (4.1) without the multi-scale Smagorinsky term c', that results in a pure projection-stabilized FEM. In this case, the parameter $\overline{\nu}_{T|_K}^n$ does not appear in the definition of the stabilization coefficients. In the sequel, we call STAB this variant of method (4.1).

Afterwards, we further integrate in parallel the numerical schemes either with no-slip boundary conditions and wall-law boundary conditions, within another 1250 time steps, in order to collect statistics and perform a comparison. We choose to apply wall-law boundary conditions only to STAB and VMS-S method (the latter is the model that gives the most promising results when the multi-scale Smagorinsky term c' is taken into account). We consider the logarithmic wall-law of Prandtl and Von Kármán (2.7), where we fix the computational boundary at $y^+ = 11.5$, and we use a uniform mesh with 12 grid-lines in wall-normal direction, neglecting the use of Van Driest damping too. This permits to avoid

the quite costly calculation of the flow near the walls, reducing the number of d.o.f. to 25 600 for each scalar variable, with a saving in computing time of about 34% compared with the use of no-slip boundary conditions. Note that before the flow becomes quasi-stationary, the value of u_τ changes a lot in time, and this implies a dynamic development of the boundary layer thickness, due to the definition of y^+. This requires a dynamic adaptation in the use of wall laws. Here, we choose a simpler procedure, letting the flow develop until reaching a stable configuration before applying wall laws in a static way.

- Numerical results.

We consider the temporal evolution of the normalized mean wall-shear stress:

$$\langle \tau^* \rangle(t) = \frac{\langle \tau \rangle(t)}{\nu} = \frac{\partial \langle u_1 \rangle}{\partial y}(\pm 1; t),$$

where $\langle \cdot \rangle$ indicates in this case averaging over the homogeneous directions. We have that, when a (quasi-)steady state is reached (at half of simulation), this mean quantity oscillates (in modulus) around 180 for all models, as indicated by the corresponding temporal averaged (from $t = 5$ to $t = 10$) values. These values have been used to compute for all methods the actual value of u_τ, subject to:

$$u_\tau = \left[\frac{\nu}{2} \frac{1}{N/2} \sum_{n=N/2}^{N-1} \left(\frac{\partial \langle u_1 \rangle}{\partial y}(-1; t_n) - \frac{\partial \langle u_1 \rangle}{\partial y}(+1; t_n) \right) \right]^{1/2}, \quad N = \#\text{ time steps} = 1\,250.$$

The simulated friction velocity u_τ (computed as the average of the computed friction velocities at both walls) is reported in Table 1, together with the corresponding computed Re_τ for all methods. We note that the friction velocity u_τ is within 0.2%-4.1% of the nominal value $u_\tau = 1$, and, as a result, so is the actual Re_τ.

	Nominal $Re_\tau = 180$	
Methods	Computed u_τ	Computed Re_τ
VMS-S	0.9887	177.966
VMS-B	0.9594	172.692
SMA	0.9977	179.586
STAB	1.0024	180.432

Table 1:
Computed u_τ and Re_τ.

Hereafter, we denote by $\langle \cdot \rangle$ the mean values and by $\widetilde{\cdot}$ the respective fluctuations, where mean values are obtained averaging over all time steps of the statistical period as well as over the homogeneous directions. In Figure 2, we show the mean stream-wise velocity profile $\langle u_1 \rangle$ (first-order statistic), normalized by the computed u_τ, in wall coordinates y^+. As usual, only half of the channel width is illustrated (i.e., the upper half-width here, ranging from $y = 0$ to $y = 1$). According to the definition of the wall coordinate y^+, the upper wall is located at $y^+ = 0$ and the channel center at $y^+ = u_\tau/\nu \approx 180$.

In particular, the displayed mean stream-wise velocity profiles are obtained by using both no-slip boundary conditions (for all methods) and wall-law boundary conditions (for VMS-S and STAB methods), and a comparison is performed with DNS data [46] and the numerical results of Akkerman [1]. Note that the DNS data so as the RB-VMS results of

Akkerman are obtained by the standard approach that uses no-slip boundary conditions at the walls. Actually, the grid resolution seems to be too coarse to reproduce exactly the DNS profile, so that in any case we have an over-estimation of the DNS data. Anyway, the results show an acceptable agreement with the fine DNS, even with the very coarse basic discretization at hand (4 times coarser than the DNS one, since we are using a quadratic discretization). The profiles obtained with the wall-law boundary conditions starting from $y^+ = 11.5$ are simply extended linearly up to the wall located at $y^+ = 0$. We are entitled to do so, because in this case the leading component of the velocity is the stream-wise velocity, so that we can "identify" the friction non-dimensional velocity u^+, defined in (2.6), by $\langle u_1 \rangle / u_\tau$. We display in Table 2 (first column) the deviation $e_0^{\langle u_1 \rangle}$ for the mean stream-wise velocity profile from the respective DNS data in a normalized discrete L^2-norm subject to:

$$e_0^{\langle u_1 \rangle} = \left[\frac{\displaystyle\int_{y^+=0}^{y^+=180} |\langle u_1 \rangle_h^+ - \langle u_1 \rangle_{DNS}^+|^2 \, dy^+}{\displaystyle\int_{y^+=0}^{y^+=180} |\langle u_1 \rangle_{DNS}^+|^2 \, dy^+} \right]^{1/2} . \tag{4.4}$$

We can observe as all methods give similar errors levels between 11% and 24%.

Methods	$e_0^{\langle u_1 \rangle}$ $(y^+ \in [0, 180])$	$e_0^{\sqrt{\langle \tilde{u}_1^2 \rangle}}$ $(y^+ \in [30, 180]$, inertial layer)
VMS-S (NO-SLIP BC)	0.1141	0.2320
VMS-S (WALL-LAW BC)	0.1734	0.2094
VMS-B (NO-SLIP BC)	0.1786	0.3341
SMA (NO-SLIP BC)	0.1260	0.3123
STAB (NO-SLIP BC)	0.1791	0.3776
STAB (WALL-LAW BC)	0.2373	0.2187
RB-VMS (Akkerman)	0.2221	0.6104

Table 2:
L^2-norm of the deviation from the DNS profiles for the stream-wise velocity.

To investigate more in detail statistical properties of this wall-bounded turbulence test, we plot second-order statistics as measure of turbulence intensities, by using either no-slip (for all methods) and wall-law (for VMS-S and STAB methods) boundary conditions. Figure 3 displays the normalized (by the computed u_τ) r.m.s. values of velocity fluctuations $\sqrt{\langle \tilde{u}_i^2 \rangle} = \left[\langle u_i^2 \rangle - \langle u_i \rangle^2 \right]^{1/2}$ $(i = 1, 2, 3)$ in wall coordinates y^+ at the upper half-width of the channel. If we compare with DNS data the various methods tested with no-slip boundary conditions, we can see slight differences for the curves associated to wall-normal and span-wise velocities, while the curve related to stream-wise velocity shows a noticeable over-prediction. We can also observe as for the r.m.s. values, the results obtained by the application of wall laws are only meaningful for the stream-wise component of the velocity, that is the leading one. Note that in this case the related curve starts at $y^+ = 11.5$, since the computational domain starts at $y^+ = 11.5$, and no extension is possible, as for the mean stream-wise velocity. However, a comparison with the other curves is possible starting from the first interior node at $y^+ \approx 30$, i.e. in the so-called *inertial layer*, as we could

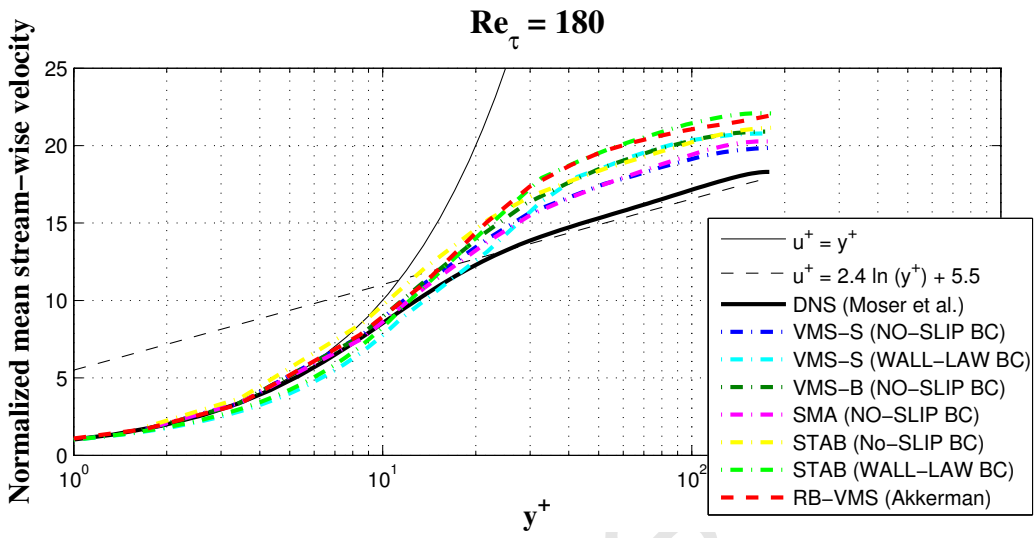

Figure 2:
Normalized mean stream-wise velocity profiles in wall coordinates y^+.

physically expect. Indeed, the inertial layer is where the logarithmic approximation of the friction-velocity u^+ is more accurate (see Figure 2). Actually, the best approximation of the r.m.s. stream-wise velocity fluctuation in the inertial layer is effectively given by the use VMS-S method with wall-laws, as shown quantitatively in Table 2 (second column), where the normalized discrete L^2-norm of the deviation from the DNS profile is computed, analogously to formula (4.4). Nevertheless, the results for the other "minor" velocity components are not acceptable compared with the DNS data at hand. In particular, this is true for the wall-normal component of the velocity, as in this case the model itself contemplates the imposition of a null wall-normal velocity at the fictitious boundary of the resulting reduced computational domain [see the boundary condition $\mathbf{u}\cdot\mathbf{n}=0$ on Γ_n in problem (2.1)], that is not expected by the use of standard no-slip boundary conditions.

This consideration obviously influences also the behavior of the Reynolds shear stress $R_{x,y}=\langle\tilde{u}_1\tilde{u}_2\rangle=\langle u_1u_2\rangle-\langle u_1\rangle\langle u_2\rangle$, where the wall-normal velocity trivially interferes. The Reynolds shear stress is plotted in Figure 4 in global coordinates y, and normalized by the computed friction velocity squared u_τ^2. Anyway, qualitatively we can observe that for all methods the Reynolds shear stress is antisymmetric, almost vanishes at the center of the channel ($y=0$), and presents a linear trend. This also indicates that a statistically steady state is already reached (Cf. [43]). If we compare with the DNS results of Moser et al. [46], the curves related to the use of no-slip boundary conditions at the walls are quite close.

Table 3 provides a quantitative picture for errors levels related to second-order statistics when the standard no-slip boundary conditions at the physical walls are incorporated in the various methods. Again, the VMS-S method is in general more in agreement with the DNS data.

Figure 5 shows the stream-wise velocity contours at different instants in time, computed by the VMS-S method employing wall-law boundary conditions. Note the presence of turbulent structures (velocity fluctuations) on the wall-normal boundary inside the boundary layer (top surfaces), and as the flow becomes more homogenous as time increases.

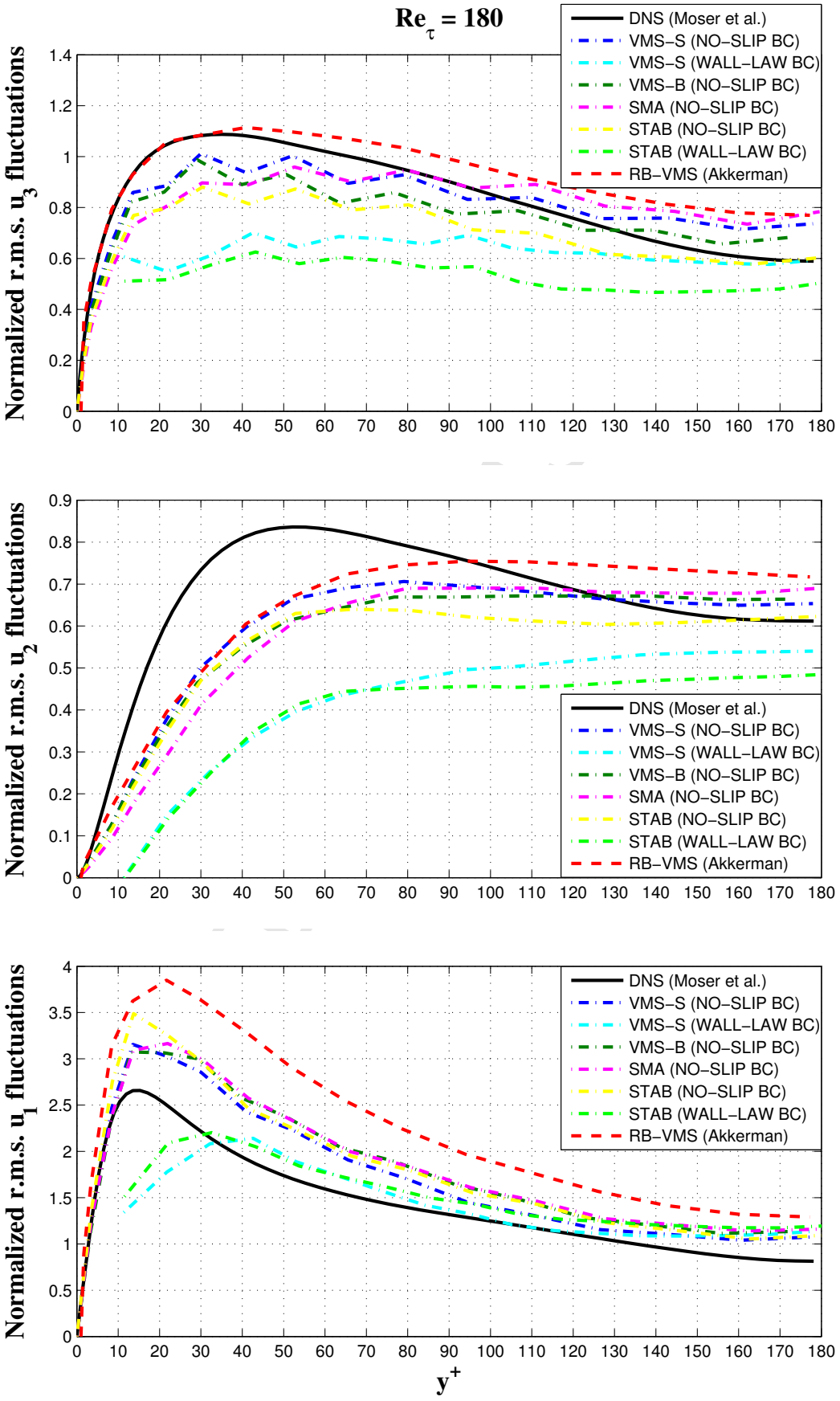

Figure 3:
Normalized r.m.s. velocity fluctuations profiles in wall coordinates y^+.

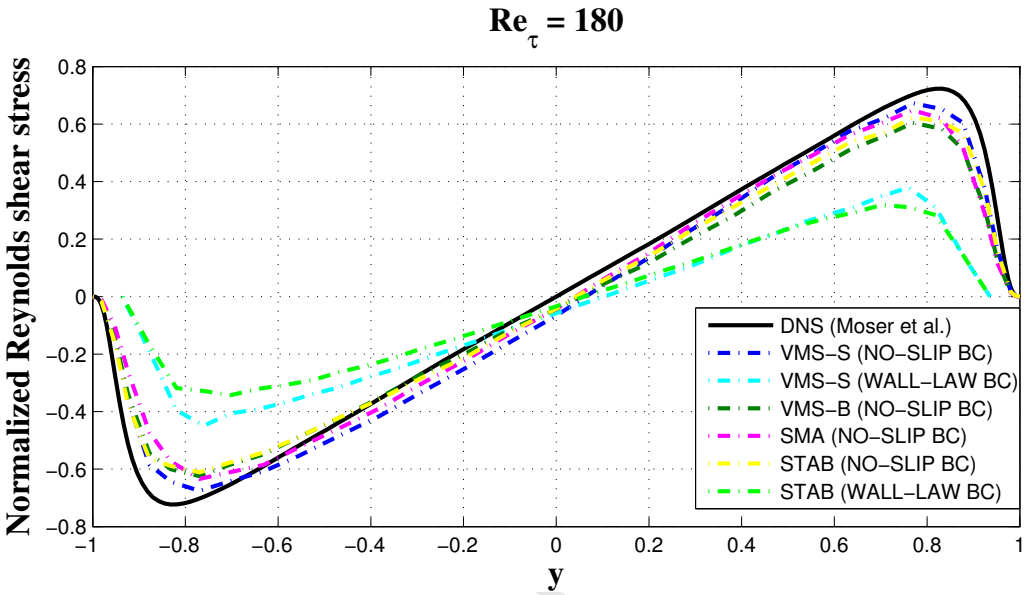

Figure 4:
Normalized Reynolds shear stress in global coordinates y.

Methods	$e_0^{\sqrt{\langle \tilde{u}_1^2 \rangle}}$	$e_0^{\sqrt{\langle \tilde{u}_2^2 \rangle}}$	$e_0^{\sqrt{\langle \tilde{u}_3^2 \rangle}}$	$e_0^{\langle \tilde{u}_1 \tilde{u}_2 \rangle}$
VMS-S (NO-SLIP BC)	0.2252	0.1652	0.1108	0.1162
VMS-B (NO-SLIP BC)	0.2881	0.2018	0.1246	0.1706
SMA (NO-SLIP BC)	0.3002	0.2236	0.1597	0.1249
STAB (NO-SLIP BC)	0.3781	0.2536	0.1955	0.1708
RB-VMS (Akkerman)	0.5694	0.1753	0.1331	-

Table 3:
L^2-norm of the deviation from the DNS profiles for the second-order statistics.

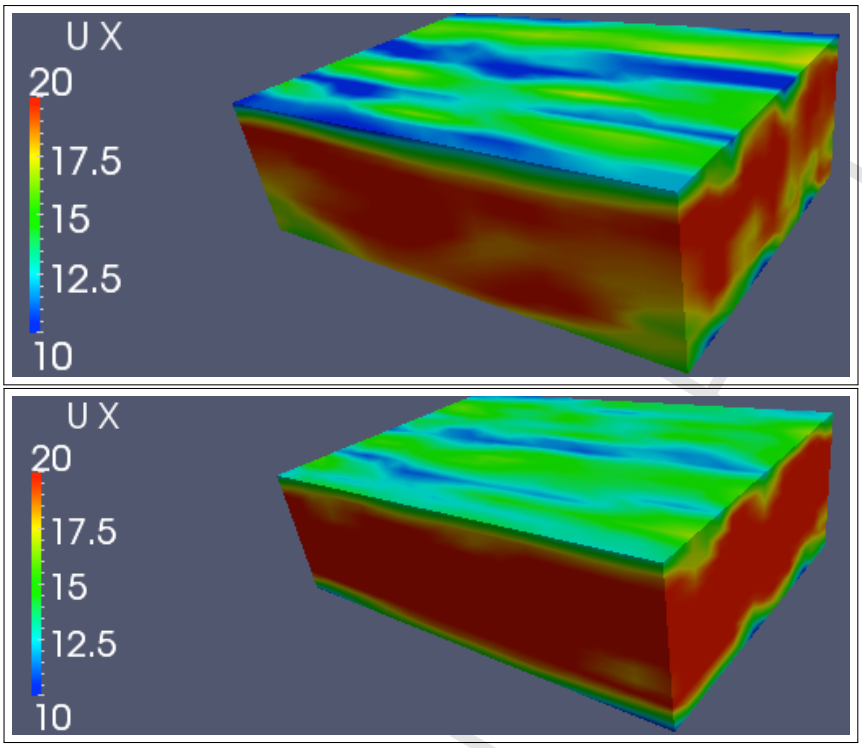

Figure 5:
Snapshot of stream-wise velocity contours at $t = 5$ (top) and $t = 10$ (bottom).

We highlight also some considerations on the computational cost corresponding to the various methods. The computing times related to the statistical period from $t = 5$ to $t = 10$ time units (1 250 time steps) for all methods are given in Table 4. These are referred to the sequential execution of the numerical code on a same machine. It can be seen that effectively the use of wall laws for VMS-S method provides a significant reduction of the computing time, of about 34%, while the CPU time of both VMS approaches is comparable with the one of the standard Smagorinsky approach, that saves at most a 4% of computing time. Also, the CPU time for STAB method is comparable with the computing times of the other methods in which the multi-scale Smagorinsky term is added, and again the use of wall laws provides a reduction of the computing time, of about 35%.

5 Conclusions

We have developed stabilized projection-based FE-VMS formulations of the incompressible Navier-Stokes equations incorporating wall-law boundary conditions in combination with inflow boundary conditions. We have performed the numerical analysis of the model introduced, proving stability and convergence for flows with minimal regularity. We have replaced the lacking density results by smooth functions by an ad-hoc internal approximation result by finite elements. We also have proved the asymptotic energy balance that holds for flows slightly smoother. Further, we have proved that the model is useful to solve both smooth and turbulent flows. Smooth flows are solved with optimal accuracy, as confirmed by numerical simulations too.

The numerical experiments on a turbulent channel flow confirm on one hand that the

Methods	CPU time
VMS-S (NO-SLIP BC)	398 207 (134)
VMS-S (WALL-LAW BC)	297 524 (100)
VMS-B (NO-SLIP BC)	401 128 (135)
SMA (NO-SLIP BC)	389 260 (131)
STAB (NO-SLIP BC)	369 872 (135)
STAB (WALL-LAW BC)	273 714 (100)

Table 4:
Computing times (in seconds); in parentheses: percentage to computing time with VMS-S (WALL-LAW BC).

application of wall-law boundary conditions could provide (at least for the leading streamwise component of the velocity) similar results to those obtained by the standard approach based on the use of no-slip boundary conditions, a refined mesh towards the walls and the Van Driest damping improvement, with a noticeable reduced computational cost. On another hand, they show that the VMS-S method gives quite good results for both first and second-order statistics, in the worst condition of a very coarse basic discretization. Note that when the multi-scale Smagorinsky term is neglected (STAB method), we obtain worse results, even if they are quite close to the ones obtained by adding the sub-grid eddy viscosity. Indeed, STAB method is not strongly consistent, and the addition of the multi-scale Smagorinsky term helps to counter-balance the consistency error. The numerical results clarify that the differences are due to the lower numerical diffusion of the STAB method, and that VMS models are more accurate due to the turbulent diffusion term.

Summarizing, the proposed VMS-S method provides a good compromise between accuracy and computational complexity, which is an important feature in the context of its practical performances.

Appendix

Error estimates

We derive error estimates for the VMS-S discretization (2.15) for diffusion-dominated flows. The interest of this analysis is to highlight the fact that the VMS-S method proposed may be used to approximate both laminar and turbulent flows. About the former, if they are regular enough, we obtain convergence of optimal order, and the order decreases with the regularity. As a consequence, we also obtain an asymptotic energy balance of the system for slightly smooth flows, as stated in Subsection 3.4 in the body of the paper. Similar error estimates may be obtained in a more general framework, when the solution of Navier-Stokes equations is located in a branch of non-singular Reynolds numbers, in the sense that at these Reynolds numbers there are no bifurcations to more complex flows (Cf. [10, 11, 12]).

We start by setting a condition that ensures the uniqueness of solutions of the steady Navier-Stokes equations (2.15).

Theorem 5.1. *Assume that:*

$$2\nu > \beta(2\mathcal{K} + \|D(\mathbf{U}_D)\|_{0,2,\Omega}), \tag{5.1}$$

where $\mathcal{K}$ is the quantity defined by (3.21), and:

$$\beta := \sup_{\mathbf{z},\mathbf{v},\mathbf{w}\in\mathbf{W}(\Omega)} \frac{b(\mathbf{z};\mathbf{v},\mathbf{w})}{\|D(\mathbf{z})\|_{0,2,\Omega}\,\|D(\mathbf{v})\|_{0,2,\Omega}\,\|D(\mathbf{w})\|_{0,2,\Omega}}.$$

Then, the solution of the steady Navier-Stokes equations (2.2) is unique.

Remark 5.2. *The condition (5.1) means that the flow is diffusion-dominated. The viscosity ν is large enough to balance the convection effects relatively to the data $\mathbf{f}$ and $\mathbf{U}_D$.*

A rather standard but quite lengthy and technical error analysis (that we skip for brevity) proves that (Cf. [50]):

Theorem 5.3. *Assume that Hypothesis 2.5 and estimate (5.1) hold, and that, for smooth enough data, the (unique) solution $(\mathbf{u},p)$ of the steady Navier-Stokes equations (2.15) has augmented regularity, i.e. $(\mathbf{u},p)\in[H^{s+1}(\Omega)]^d\times H^s(\Omega)$, $2\leq s\leq l$. Then, the following error estimates for a solution $(\mathbf{u}_h,p_h)$ of the VMS-S method (2.15) hold:*

$$\|D(\mathbf{u}-\mathbf{u}_h)\|_{0,2,\Omega}+\|p-p_h\|_{0,2,\Omega}\leq C\left(h^s+h^{2-d/2+2\eta}\right), \tag{5.2}$$

for some constant C inversely proportional to ν and independent of h, and $\eta\leq(l-1)$ if Π_h takes values in $\overline{\mathbf{Y}}_h$ defined by (2.12), while $\eta\leq l$ if Π_h takes values in $\overline{\mathbf{Y}}_h$ defined by (2.13), l denoting the degree of the polynomial interpolation.

Remark 5.4. *We note that, in any case, the convergence order of the VMS-S method (2.15) is optimal with respect to the polynomial interpolation for laminar smooth flows.*

Decreasing the regularity of the solution $(\mathbf{u},p)$ of the steady Navier-Stokes equations (at most) to $[H^2(\Omega)]^d\times H^1(\Omega)$ implies that the convergence order of the VMS-S method is limited to one, due to the estimate of the pressure stabilizing term. However, this slightly augmented regularity already guarantees the strong convergence of the VMS-S method.

Acknowledgements: Research partially supported by the Spanish Government project MTM2012-36124-C02-01.

References

[1] I. Akkerman. *Adaptative variational multiscale formulations using the discrete Germano approach.* PhD thesis, Delft University of Technology, 2009.

[2] Y. Bazilevs, V. M. Calo, J. A. Cottrell, T. J. R. Hughes, A. Reali, and G. Scovazzi. Variational multiscale residual-based turbulence modeling for large eddy simulation of incompressible flows. *Comput. Methods Appl. Mech. Engrg.*, 197(1-4):173–201, 2007.

[3] Y. Bazilevs, C. Michler, V. M. Calo, and T. J. R. Hughes. Weak Dirichlet boundary conditions for wall-bounded turbulent flows. *Comput. Methods Appl. Mech. Engrg.*, 196(49-52):4853–4862, 2007.

[4] Y. Bazilevs, C. Michler, V. M. Calo, and T. J. R. Hughes. Isogeometric variational multiscale modeling of wall-bounded turbulent flows with weakly enforced boundary conditions on unstretched meshes. *Comput. Methods Appl. Mech. Engrg.*, 199(13-16):780–790, 2010.

[5] C. Bernardi, T. Chacón Rebollo, and D. Yakoubi. Finite element discretization of the Stokes and Navier-Stokes equations with boundary conditions on the pressure. Submitted (http://hal.upmc.fr/hal-00961653), 2014.

[6] C. Bernardi, Y. Maday, and F. Rapetti. *Discrétisations variationnelles de problèmes aux limites elliptiques*, volume 45 of *Mathématiques & Applications*. Springer-Verlag, 2004.

[7] L. C. Berselli, T. Iliescu, and W. J. Layton. *Mathematics of large eddy simulation of turbulent flows*. Scientific Computation. Springer-Verlag, Berlin, 2006.

[8] M. Braack and E. Burman. Local projection stabilization for the Oseen problem and its interpretation as a variational multiscale method. *SIAM J. Numer. Anal.*, 43(6):2544–2566, 2006.

[9] H. Brezis. *Analyse fonctionnelle: Théorie et applications*. Masson, 1983.

[10] F. Brezzi, J. Rappaz, and P.-A. Raviart. Finite-dimensional approximation of nonlinear problems. I. Branches of nonsingular solutions. *Numer. Math.*, 36(1):1–25, 1980/81.

[11] F. Brezzi, J. Rappaz, and P.-A. Raviart. Finite-dimensional approximation of nonlinear problems. II. Limit points. *Numer. Math.*, 37(1):1–28, 1981.

[12] F. Brezzi, J. Rappaz, and P.-A. Raviart. Finite-dimensional approximation of nonlinear problems. III. Simple bifurcation points. *Numer. Math.*, 38(1):1–30, 1981/82.

[13] E. Burman. Interior penalty variational multiscale method for the incompressible Navier-Stokes equation: monitoring artificial dissipation. *Comput. Methods Appl. Mech. Engrg.*, 196(41-44):4045–4058, 2007.

[14] T. Chacón Rebollo. A term by term stabilization algorithm for finite element solution of incompressible flow problems. *Numer. Math.*, 79(2):283–319, 1998.

[15] T. Chacón Rebollo. An analysis technique for stabilized finite element solution of incompressible flows. *M2AN Math. Model. Numer. Anal.*, 35(1):57–89, 2001.

[16] T. Chacón Rebollo, M. Gómez Mármol, V. Girault, and I. Sánchez Muñoz. A high order term-by-term stabilization solver for incompressible flow problems. *IMA J. Numer. Anal.*, 33(3):974–1007, 2013.

[17] T. Chacón Rebollo, M. Gómez Mármol, and M. Restelli. Numerical analysis of penalty stabilized finite element discretizations of evolution Navier-Stokes equation. *J. Sci. Comput.*, 61(1):1–28, 2014.

[18] T. Chacón Rebollo, M. Gómez Mármol, and S. Rubino. Derivation of the Smagorinsky model from a Galerkin discretization. In *Mascot11 Proc.*, volume 17 of *IMACS Series in Comp. and Appl. Math.*, pages 61–70, 2013.

[19] T. Chacón Rebollo, M. Gómez Mármol, and S. Rubino. TurboMathS: a FreeFem++ numerical code for VMS turbulence models. Technical report, Research Group "Modelado Matemático y Simulación de Sistemas Medioambientales", University of Seville, 2014.

[20] T. Chacón Rebollo, F. Hecht, M. Gómez Mármol, G. Orzetti, and S. Rubino. Numerical approximation of the Smagorinsky turbulence model applied to the primitive equations of the ocean. *Math. Comput. Simulation*, 99:54–70, 2014.

[21] T. Chacón Rebollo and R. Lewandowski. A variational finite element model for large-eddy simulations of turbulent flows. *Chin. Ann. Math. Ser. B*, 34(5):667–682, 2013.

[22] T. Chacón Rebollo and R. Lewandowski. *Mathematical and numerical foundations of turbulence models and applications*. Birkhäuser, 2014.

[23] H. Choi and P. Moin. Effects of the computational time step on numerical solutions of turbulent flow. *J. Comput. Phys.*, 113(1):1–4, 1994.

[24] R. Codina. Comparison of some finite element methods for solving the diffusion-convection-reaction equation. *Comput. Methods Appl. Mech. Engrg.*, 156(1-4):185–210, 1998.

[25] R. Codina. Stabilization of incompressibility and convection through orthogonal sub-scales in finite element methods. *Comput. Methods Appl. Mech. Engrg.*, 190(13-14):1579–1599, 2000.

[26] R. Codina. A stabilized finite element method for generalized stationary incompressible flows. *Comput. Methods Appl. Mech. Engrg.*, 190(20-21):2681–2706, 2001.

[27] R. Codina, J. Principe, and S. Badia. Dissipative structure and long term behavior of a finite element approximation of incompressible flows with numerical subgrid scale modeling. In *Multiscale methods in computational mechanics*, volume 55 of *Lect. Notes Appl. Comput. Mech.*, pages 75–93. Springer, 2011.

[28] J. W. Deardorff. A numerical study of three-dimensional turbulent channel flow at large Reynolds numbers. *J. Fluid Mech.*, 41:453–465, 1970.

[29] T. Dubois, F. Jauberteau, and R. Temam. *Dynamic multilevel methods and the numerical simulation of turbulence*. Cambridge University Press, 1999.

[30] V. Gravemeier. Scale-separating operators for variational multiscale large eddy simulation of turbulent flows. *J. Comput. Phys.*, 212(2):400–435, 2006.

[31] F. Hecht. New development in freefem++. *J. Numer. Math.*, 20(3-4):251–265, 2012.

[32] C. O. Horgan. Korn's inequalities and their applications in continuum mechanics. *SIAM Rev.*, 37(4):491–511, 1995.

[33] T. J. R. Hughes, G. R. Feijóo, L. Mazzei, and J.-B. Quincy. The variational multiscale method—a paradigm for computational mechanics. *Comput. Methods Appl. Mech. Engrg.*, 166(1-2):3–24, 1998.

[34] T. J. R. Hughes, L. Mazzei, and K. E. Jansen. Large eddy simulation and the variational multiscale method. *Comput. Vis. Sci.*, 3(1-2):47–59, 2000.

[35] T. J. R. Hughes, L. Mazzei, A. A. Oberai, and A. Wray. The multiscale formulation of large eddy simulation: Decay of homogeneous isotropic turbulence. *Phys. Fluids*, 13(2):505–512, 2001.

[36] T. J. R. Hughes, A. A. Oberai, and L. Mazzei. Large eddy simulation of turbulent channel flows by the variational multiscale method. *Phys. Fluids*, 13(6):1784–1799, 2001.

[37] T. Iliescu and P. F. Fischer. Large eddy simulation of turbulent channel flows by the rational large eddy simulation model. *Phys. Fluids*, 15(10):3036–3047, 2003.

[38] V. John. On large eddy simulation and variational multiscale methods in the numerical simulation of turbulent incompressible flows. *Appl. Math.*, 51(4):321–353, 2006.

[39] V. John and S. Kaya. A finite element variational multiscale method for the Navier-Stokes equations. *SIAM J. Sci. Comput.*, 26(5):1485–1503, 2005.

[40] V. John, S. Kaya, and A. Kindl. Finite element error analysis for a projection-based variational multiscale method with nonlinear eddy viscosity. *J. Math. Anal. Appl.*, 344(2):627–641, 2008.

[41] V. John and A. Kindl. Numerical studies of finite element variational multiscale methods for turbulent flow simulations. *Comput. Methods Appl. Mech. Engrg.*, 199(13-16):841–852, 2010.

[42] W. P. Jones and M. Wille. Large eddy simulation of a jet in a cross-flow. In *10th Symposium on Turbulent Shear Flows*, volume 4, pages 1–6, 1995.

[43] J. Kim, P. Moin, and R. Moser. Turbulence statistics in fully developed channel flow at low Reynolds number. *J. Fluid Mech.*, 177:133–166, 1987.

[44] J. L. Lions. *Quelques méthodes de résolution des problèmes aux limites non linéaires.* Dunod, 2002.

[45] P. Moin and J. Kim. Numerical investigation of turbulent channel flow. *J. Fluid Mech.*, 118:341–377, 1982.

[46] R. Moser, J. Kim, and N. N. Mansour. Direct numerical simulation of turbulent channel flow up to $Re_\tau = 590$. *Phys. Fluids*, 11(4):943–945, 1999.

[47] C. Parés. Existence, uniqueness and regularity of solution of the equations of a turbulence model for incompressible fluids. *Appl. Anal.*, 43(3-4):245–296, 1992.

[48] C. Parés. Approximation de la solution des équations d'un modèle de turbulence par une méthode de Lagrange-Galerkin. *Rev. Mat. Apl.*, 15(2):63–124, 1994.

[49] L. Prandtl. Über die ausgebildeten Turbulenz. *Zeitschrift für angewandte Mathematik und Mechanik*, 5:136–139, 1925.

[50] S. Rubino. *Numerical modeling of turbulence by Richardson number-based and VMS models.* PhD thesis, Univeristy of Seville, 2014.

[51] Y. Saad and M. H. Schultz. GMRES - A generalized minimal residual algorithm for solving nonsymmetric linear systems. *SIAM J. Sci. Stat. Comp.*, 7(3):856–869, 1986.

[52] R. L. Scott and S. Zhang. Finite element interpolation of non-smooth functions satisfying boundary conditions. *Math. Comput.*, 54(190):483–493, 1990.

[53] J. Smagorinsky. General circulation experiment with the primitive equations: I. The basic experiment. *Mon. Weather Rev.*, 91(3):99–164, 1963.

[54] D. B. Spalding. A single formula for the "law of the wall". *J. Appl. Mech.*, 28(3):455–458, 1961.

[55] E. R. Van Driest. On turbulent flow near a wall. *J. Aerosp. Sci.*, 23(11):1007–1011, 1956.

[56] R. Verfürth. Finite element approximation of steady Navier-Stokes equations with mixed boundary conditions. *RAIRO Modél. Math. Anal. Numér.*, 19(3):461–475, 1985.

[57] R. Verfürth. Finite element approximation of incompressible Navier-Stokes equations with slip boundary condition. *Numer. Math.*, 50(6):697–721, 1987.

[58] T. Von Kármán. Mechanische Ähnlichkeit und Turbulenz. *Nachr. Ges. Wiss. Gottingen, Math. Phys. Klasse*, 58, 1930.